Sequence of Events Underlying the Allosteric Transition of Rod Cyclic Nucleotide–gated Channels

Elizabeth R. Sunderman and William N. Zagotta

From the Department of Physiology and Biophysics, Howard Hughes Medical Institute, University of Washington, Seattle, Washington 98195

ABSTRACT Activation of cyclic nucleotide–gated (CNG) ion channels involves a conformational change in the channel protein referred to as the allosteric transition. The amino terminal region and the carboxyl terminal cyclic nucleotide–binding domain of CNG channels have been shown to be involved in the allosteric transition, but the sequence of molecular events occurring during the allosteric transition is unknown. We recorded single-channel currents from bovine rod CNG channels in which mutations had been introduced in the binding domain at position 604 and/or the rat olfactory CNG channel amino terminal region had been substituted for the bovine rod amino terminal region. Using a hidden Markov modeling approach, we analyzed the kinetics of these channels activated by saturating concentrations of cGMP, cIMP, and cAMP. We used thermodynamic mutant cycles to reveal an interaction during the allosteric transition between the purine ring of the cyclic nucleotides and the amino acid at position 604 in the binding site. We found that mutations at position 604 in the binding domain alter both the opening and closing rate constants for the allosteric transition, indicating that the interactions between the cyclic nucleotide and this amino acid are partially formed at the time of the transition state. In contrast, the amino terminal region affects primarily the closing rate constant for the allosteric transition, suggesting that the state-dependent stabilizing interactions between amino and carboxyl terminal regions are not formed at the time of the transition state for the allosteric transition. We propose that the sequence of events that occurs during the allosteric transition involves the formation of stabilizing interactions between the purine ring of the cyclic nucleotide and the amino acid at position 604 in the binding domain followed by the formation of stabilizing interdomain interactions.

KEY WORDS: electrophysiology • ion channel gating • kinetics • cyclic GMP • open probability

introduction

Cyclic nucleotide-gated (CNG)[1] ion channels of retinal rod photoreceptors are exquisitely sensitive molecular detectors of the cyclic nucleotide concentration. The binding of cyclic nucleotide triggers an allosteric conformational change in the channel protein that opens the channel pore. In the preceding paper (Sunderman and Zagotta, 1999), we showed that interactions between the purine ring of the cyclic nucleotide and the binding domain are partially formed at the time of the transition state for the allosteric transition. These interactions serve to reduce the transition-state energy and stabilize the activated conformation of the channel relative to the closed state. In this paper, we extend our analysis of the kinetics of the allosteric transition of bovine rod (BROD) CNG channels by determining the effects on the allosteric transition of mutations at position 604 in the binding domain and of substitution of the olfactory amino terminal region. These experiments provide insight into the sequence of molecular events that occur during the conformational change involved in channel activation.

CNG channels contain, in their intracellular carboxyl terminal region, a domain with significant sequence similarity to the cyclic nucleotide–binding domain of a number of other cyclic nucleotide–binding proteins, including cGMP- and cAMP-dependent protein kinases and *Escherichia coli* catabolite gene activator protein (CAP) (Kaupp et al., 1989). CAP is a cAMP-activated transcription factor whose structure, while bound to cAMP, has been determined by x-ray crystallography to 2.5 Å resolution (McKay and Steitz, 1981; Weber and Steitz, 1987). The structure of the cyclic nucleotide–binding site of CAP consists of eight β strands that form a β roll structure, followed by two α helices, designated the B helix and C helix. Each cAMP molecule binds in the anti configuration with the ribose and cyclic phosphate binding to the pocket formed by the β roll and with the N6 hydrogen of adenine hydrogen bonding with a threonine at position T127 and a serine at position S128 on the opposite subunit (Weber and Steitz, 1987).

Address correspondence to William N. Zagotta, Department of Physiology and Biophysics, Box 357290, University of Washington, Seattle, Washington 98195-7290. Fax: 206-543-0934; E-mail: zagotta@u.washington.edu

[1]*Abbreviations used in this paper:* BROD, bovine rod; CAP, catabolite gene activator protein; CNG, cyclic nucleotide–gated; HMM, hidden Markov model.

Rod CNG channels differ markedly in their apparent affinities for cGMP, cIMP, and cAMP (Varnum et al., 1995). To account for the selectivity for cGMP over cAMP in the rod CNG channel, Varnum et al. (1995) proposed that the cyclic nucleotides bind in the anti configuration (Fig. 1). For the case of cGMP, a pair of hydrogen bonds could then form between the N1 and N2 hydrogens of the guanine ring of cGMP and the aspartate residue at position 604 in the binding site (Varnum et al., 1995). Cyclic AMP, which has an unshared pair of electrons at the N1 position, would form an unfavorable electrostatic interaction with the aspartate at position 604 and thus bind with lower affinity. Alternatively, it has also been proposed for the cGMP-dependent protein kinases and for the cGMP-gated channels that the cyclic nucleotides bind in the syn configuration, with the N2 hydrogen of guanine hydrogen bonded to a threonine residue in the β roll found primarily in cGMP-selective proteins (Altenhofen et al., 1991; Shabb et al., 1991; Kumar and Weber, 1992).

The amino terminal region of CNG channels has been shown to affect the free energy of the allosteric transition (Chen and Yau, 1994; Goulding et al., 1994; Gordon and Zagotta, 1995b). In particular, the amino terminal region of olfactory CNG channels has been shown to promote the allosteric transition. This effect of the olfactory amino terminal region is transferable to rod channels, as chimeric rod channels with the olfactory amino terminal region open more favorably, and, conversely, chimeric olfactory channels with the rod amino terminal region exhibit much less favorable opening (Goulding et al., 1994; Gordon and Zagotta, 1995b). Using in vitro protein interaction assays, specific interactions have been observed between the amino and carboxyl terminal regions of the olfactory CNG channel and between the olfactory amino terminal region and the rod carboxyl terminal region (Varnum and Zagotta, 1997). Similar results were seen with the rod amino terminal region (Gordon et al. 1997). These results indicate that the amino and carboxyl terminal regions of CNG channels bind with high affinity. Thus, conformational changes in the cyclic nucleotide–binding domain in the carboxyl terminal region could be transduced to the amino terminal region because of its close proximity and high affinity interaction. In addition, these results provide a molecular mechanism for how the gating of olfactory CNG channels can be modulated by Ca^{2+}-calmodulin (Chen and Yau, 1994; Liu et al., 1994; Varnum and Zagotta, 1997).

In this paper, we analyze the kinetic behavior of single BROD CNG channels in which mutations at amino acid position 604 in the binding domain have been introduced and/or the rat olfactory amino terminal region has been substituted for the BROD amino termi-

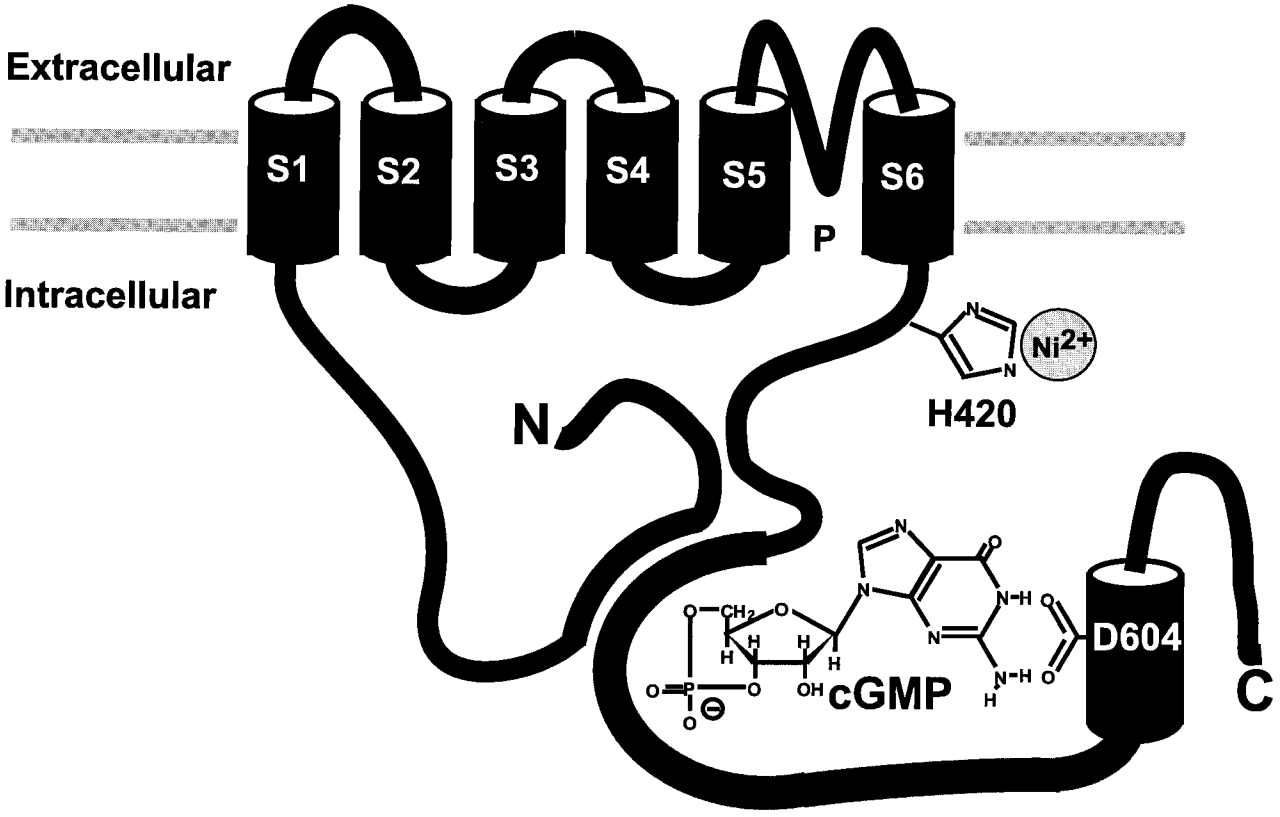

FIGURE 1. CNG channel α subunit.

nal region. These experiments test the hypothesis that a pair of hydrogen bonds forms between cGMP and D604 during the allosteric transition and probe the mechanism by which the amino terminal region affects the energetics of the allosteric transition. Using a hidden Markov model approach, we analyzed the single-channel records to determine the underlying rate constants. We used thermodynamic mutant cycle formalism to determine the coupling energies for these interactions. By comparing the free energies of the transition state for the allosteric transition relative to the closed and open state energies across mutants and cyclic nucleotides, we postulate a sequence for the molecular events that occur during the allosteric transition.

materials and methods

Oocyte preparation, cRNA transcription, and expression were carried out as described previously (Zagotta et al., 1989). Site-specific mutations were generated using oligonucleotide-directed mutagenesis and PCR and were confirmed by sequencing as described previously (Gordon and Zagotta, 1995a). Patch-clamp experiments and analysis of data were carried out as described in the preceding paper (Sunderman and Zagotta, 1999). In brief, patch-clamp experiments were performed in the inside-out conformation using an Axopatch 200B amplifier (Axon Instruments). Currents were low-pass filtered at 5 kHz (eight-pole Bessel) and sampled at 25 kHz. Recordings were made at 20–22°C. Initial pipette resistances were 5–20 MΩ. Intracellular and extracellular solutions contained 130 mM NaCl, 3 mM HEPES, and 0.2 mM EDTA, pH 7.2. For the experiments with Ni^{2+}, 1 μM Ni^{2+} was substituted for the EDTA. 500 μM niflumic acid was included in the patch pipette to reduce endogenous calcium-activated chloride currents. Intracellular solutions containing cyclic nucleotides and/or 1 μM Ni^{2+} were changed using a DAD-12 Superfusion System (Adams and List Associates Ltd.) controlled by a MRI MB-8000 PC and modified such that each solution had a separate exit port. All reagents were obtained from Sigma Chemical Co.

Fractional activations (I/I_{max}) for a particular cyclic nucleotide were calculated by dividing the current (I) in the presence of the cyclic nucleotide by the maximum current obtained in the presence of 1 μM Ni^{2+} plus the best agonist for that channel (I_{max}). The fractional activation was used to estimate the free energy change of the allosteric transition by assuming that the equilibrium constant (L) for this transition is given by: $I/I_{max} = L/(L + 1)$. Thus the standard free energy for the allosteric transition is $\Delta G^0 - RT$ in L, where R is the universal gas constant and T is the temperature.

Transition-State Theory

Conversions of rate constants to transition state energies were made according to Eyring rate theory (Eyring, 1935), which assumes that there is a quasi-equilibrium between the transition state and the ground state and that the rate of break down to product of the high energy intermediate depends on the vibrational energy of a covalent bond at room temperature. While originally proposed for chemical reactions, this theory has been applied to conformational changes in proteins and is useful because it provides an estimate of the transition state energies (Creighton, 1993). Thus $\Delta G^{\ddagger} = RT \ln(k_B T/k_{obs} h) = (17.3 - 1.35 \log k_{obs})$ kcal/mol at 22°C, where $\Delta G^{\ddagger}$ is the transition state energy, R is the universal gas constant, T is the temperature, k_B is the Boltzmann constant, k_{obs} is the observed transition rate constant, and h is Planck's constant.

results

To investigate the molecular interactions underlying the allosteric transition, we recorded macroscopic and single-channel currents from 10 BROD CNG channel constructs in which mutations were introduced at position 604 in the binding domain and/or the rat olfactory amino terminal region was substituted for the BROD amino terminal region (CHM15). The mutations at D604 included D604E (present in the mammalian olfactory α subunit), D604Q (present in the fish olfactory α subunit), D604N (present in the rod β subunit), and D604M (present in the olfactory β subunit). These constructs were expressed as homomultimers in *Xenopus laevis* oocytes, and macroscopic currents from inside-out patches at saturating concentrations of cGMP, cIMP, and cAMP are shown in Figs. 2–4, respectively.

Control of Fractional Activation by Amino Acid at Position 604

In Fig. 2 are shown representative current families elicited by voltage steps from 0 mV to between −80 and +80 mV in the presence of 16 mM cGMP, a saturating concentration for each of the 10 constructs (Varnum et al., 1995). The currents in the absence of cyclic nucleotide were subtracted from each trace. To compare the currents across experiments, each current family was normalized to the maximum current obtained at +80 mV in the presence of 1 μM Ni^{2+} and the cyclic nucleotide that best activated the channel. As can be seen in Fig. 2 A, the fractional activation for BROD with cGMP was greatest for D604, averaging 0.96 ± 0.01 (mean ± SEM, $n = 6$). The fractional activation was slightly less (0.81 ± 0.05, $n = 4$) for the conservative D604E mutation. When the amino acid at position 604 was mutated to a polar uncharged residue (D604Q or D604N), there was a dramatic reduction in the fractional activation (D604Q, 0.12 ± 0.03, $n = 4$; D605N, 0.08 ± 0.02, $n = 4$). The fractional activation further decreased to 0.03 ± 0.01 ($n = 3$) in D604M. Thus, the fractional activation decreased as the amino acid at position 604 became progressively less polar. Since saturating concentrations of cyclic nucleotide were used in all of these experiments, a reduction in fractional activation indicates that the allosteric conformational change for fully liganded channels was less favorable for the mutant channels than for the wild-type channel. The dramatic reduction in fractional activation from 0.96 for D604 down to 0.03 for D604M is a testament to the importance of D604 for the allosteric transition. This result is consistent with what has been previously reported and has been proposed to result from hydro-

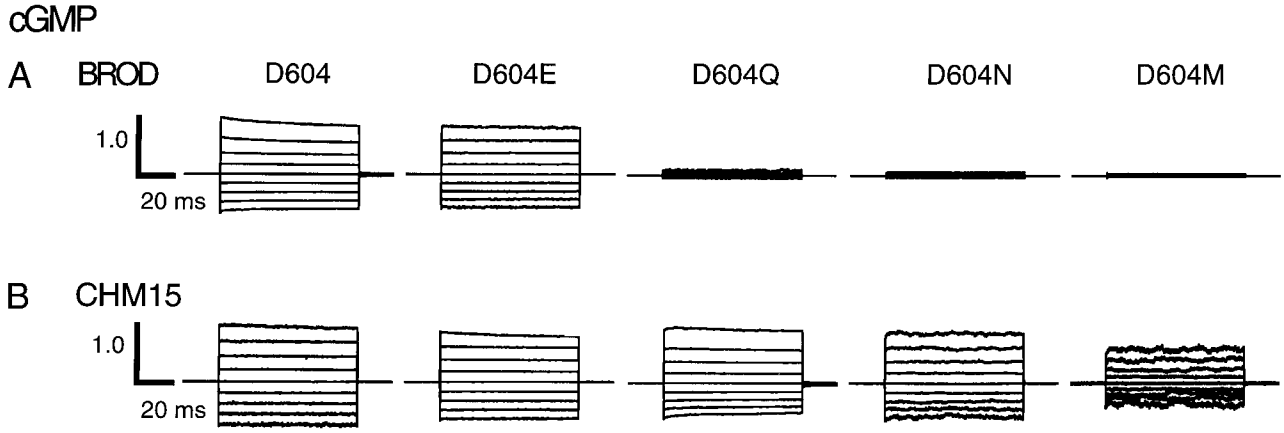

FIGURE 2. Current families for wild-type and mutant channels activated by cGMP. Current families are shown from inside-out patches excised from *Xenopus laevis* oocytes expressing BROD (A) and CHM15 (B) channels with mutations at position 604. Currents were elicited by 16 mM cGMP and voltage pulses from 0 mV to potentials between −80 and +80 mV in 20-mV steps. Leak currents in the absence of cyclic nucleotides were subtracted. The currents were normalized (using the +80-mV trace) to the maximum current obtained after Ni^{2+} potentiation (Gordon and Zagotta, 1995a) in the presence of a saturating concentration of the best agonist.

gen bonding between the carbonyl group of D604 and the guanine ring of cGMP (Varnum et al., 1995).

For comparison, the same mutations at position 604 were also studied in the CHM15 background. CHM15 is identical to the BROD construct except that the rat olfactory amino terminal region has been substituted for the BROD amino terminal region (Gordon and Zagotta, 1995b). The olfactory amino terminal region produces a more favorable free energy change for the allosteric transition of chimeric channels (Goulding et al., 1994; Gordon and Zagotta, 1995b), making the effects of mutations that dramatically decrease the ability of cyclic nucleotides to promote the allosteric transition easier to characterize at both the macroscopic and single-channel levels. In Fig. 2 B are illustrated the currents in the CHM15 background for the D604 mutants in the presence of cGMP. Again as the amino acid at position 604 was made progressively less polar, the fractional activation decreased. The fractional activities were 0.96 ± 0.02 (n = 4) for CHM15-D604, 0.98 ± 0.01 (n = 3) for CHM15-D604E, 0.90 ± 0.01 (n = 3) for CHM15-D604Q, 0.82 ± 0.02 (n = 5) for CHM15-D604N, and 0.52 ± 0.07 (n = 3) for CHM15-D604M. We interpret these results to indicate that, compared with the BROD background, the trend across constructs was similar, although the differences in fractional activation were smaller. Despite smaller effects on the fractional activations, the effects of the D604 mutations on the free energy of the allosteric transition is the same in both the BROD and CHM15 backgrounds (see Table I).

Cyclic IMP is similar in chemical structure to cGMP except that the inosine moiety lacks a 2-amino group. Therefore, different abilities of cGMP and cIMP to promote the allosteric transition should reflect the contribution of interactions of the cyclic nucleotide–binding domain of the channel with the guanine 2-amino group of cGMP to the allosteric transition. We recorded macroscopic currents from the 10 constructs activated by cIMP, and these currents are illustrated in Fig. 3, A and B, for the BROD and CHM15 backgrounds, respectively. As can be seen in this figure, the fractional activation was less for the D604Q, D604N, and D604M mutants than for D604 and D604E in both the BROD and CHM15 backgrounds. In BROD D604, the fractional activation by cIMP was only 0.60 ± 0.02 (n = 6) and, for BROD D604E, the fractional activation was slightly lower (0.41 ± 0.05, n = 4). For D604Q and D604N, the fractional activations were 0.05 ± 0.01 (n = 4) and 0.08 ± 0.02 (n = 4), respectively. For D604M, the fractional activation was 0.06 ± 0.004 (n = 4). For the CHM15 constructs, the fractional activations were 0.97 ± 0.01 (n = 4) for D604, 0.98 ± 0.01 (n = 3) for D604E, 0.73 ± 0.05 (n = 5) for D604Q, 0.84 ± 0.03 (n = 5) for D604N, and 0.71 ± 0.03 (n = 3) for D604M. Thus, mutating D604 to a polar uncharged residue (Q or N) or nonpolar uncharged residue (M) decreased the fractional activation. Compared with the effects for cGMP, the differences in fractional activation were smaller, suggesting that cIMP is less sensitive to the identity of the amino acid at position 604. This finding likely reflects cIMP's lesser potential for hydrogen bonding interactions than cGMP's. Thus, the energetic effects of mutations at position 604 would be expected to be smaller for cIMP than for cGMP.

Like cIMP, cAMP lacks a 2-amino group, but it has two other differences in the purine ring. cAMP has an amino group instead of a carbonyl group at the 6-position, and it has an unshared pair of electrons instead of a hydrogen at the 1-position. In Fig. 4 are illustrated currents activated by 16 mM cAMP. Here the pattern

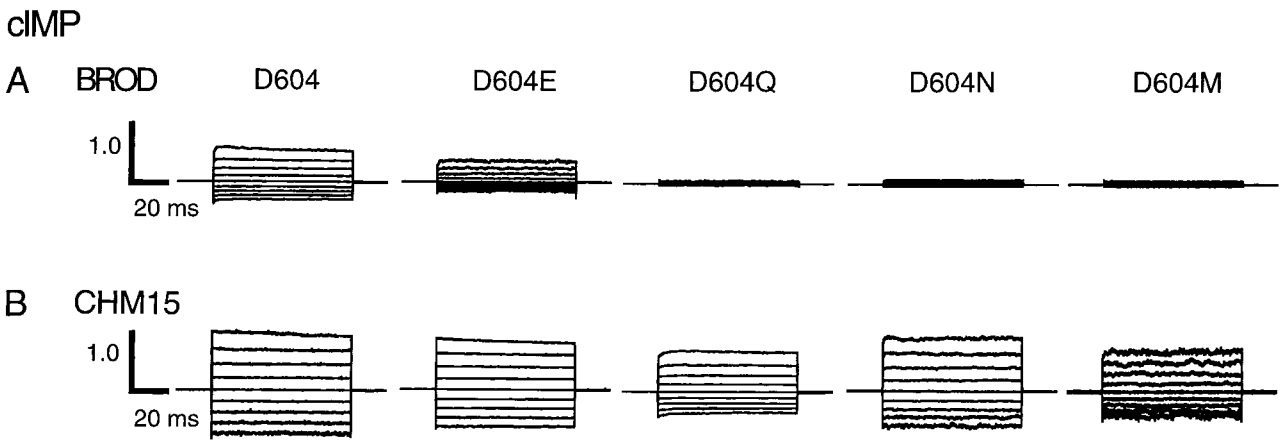

FIGURE 3. Current families for wild-type and mutant channels activated by cIMP. Current families are shown from inside-out patches excised from *Xenopus laevis* oocytes expressing BROD (A) and CHM15 (B) channels with mutations at position 604. Currents were elicited by 16 mM cIMP and voltage pulses from 0 mV to potentials between −80 and +80 mV in 20-mV steps. Leak currents in the absence of cyclic nucleotides were subtracted. The currents were normalized (using the +80-mV trace) to the maximum current obtained after Ni^{2+} potentiation (Gordon and Zagotta, 1995a) in the presence of a saturating concentration of the best agonist.

across the constructs was quite different from the pattern that was observed with cGMP and cIMP. For D604, the fractional activation was only 0.012 ± 0.002 (n = 6) or almost two orders of magnitude less than for cGMP on the same construct. For D604E, the activation was almost twice as large but still small: 0.02 ± 0.01 (n = 3). For D604Q and D604N, the activation increased to 0.05 ± 0.01 (n = 4) and 0.05 ± 0.02 (n = 4), respectively. For D604M, the fractional activation was significantly larger: 0.18 ± 0.01 (n = 3). For the CHM15 constructs, the fractional activation was 0.19 ± 0.02 (n = 4) and 0.53 ± 0.03 (n = 3) for D604 and D604E. For D604Q and D604N, the fractional activations were 0.74 ± 0.04 (n = 5) and 0.69 ± 0.03 (n = 6), respectively. For D604M, the activation was 0.90 ± 0.03 (n = 3). Thus, as the amino acid at position 604 was made progressively less polar, cAMP became a better agonist. The molecular interpretation of this result is that the reduction in the polarity of the residue at position 604 reduces the unfavorable interaction that would be expected to occur between the unshared pair of electrons at the N1 position of cAMP and a polar residue at 604. The slight improvements in the factional activations by cAMP of D604E over D604 may be related to differences in the local pKa's of aspartate and glutamate. Specifically, Gordon et al. (1996) showed that the fractional activation by cAMP on D604 improves as the pH is decreased. The cyclic nucleotide–specific pH effect disappeared when D604N was introduced, suggesting that cAMP is sensitive to the protonation state of D604. The pH dependence was proposed to result from neutralization of a negative electrostatic interaction between the negative charge on 604N and the unshared pair of electrons at the 1-position of the purine ring of cAMP. At pH 7.2, D604 would be unprotonated, but it is possible that D604E is partially protonated at pH 7.2, thereby improving the fractional activation by cAMP by removing some of the negative charge on the carboxylic acid.

Thermodynamic Mutant Cycle Analysis

To summarize the results from the macroscopic experiments, we converted the fractional activations to free energies for the allosteric transition (see MATERIALS AND METHODS) and used these energies to construct thermodynamic mutant cycles. Thermodynamic mutant cycles provide a way of separating out indirect effects of mutations on the machinery of the allosteric transition from direct interactions of the ligand with the ligand-binding domain. Thermodynamic mutant cycles have been applied to interactions between the amino acids within proteins (Carter et al., 1984; Horovitz et al., 1990; Serrano et al., 1990) and between a toxin and a voltage-dependent K^+ channel (Hidalgo and MacKinnon, 1995). We wanted to determine if the effects of mutations at 604 reflect direct interactions between D604 and the places on the purine rings where the cyclic nucleotides differ. An example of the use of thermodynamic mutant cycles is shown in Fig. 5. In Fig. 5 A, we tested for direct interaction of the amino terminal region with the purine ring of the cyclic nucleotide. The horizontal arrows reflect the effect of the amino terminal substitution on the free energy change of the allosteric transition, while the vertical arrows reflect the effect of changing cyclic nucleotide on the free energy change of the allosteric transition for the particular channel constructs. We would expect that the effect of the mutation might have two components: (a) a nonspecific component relating to indirect effects on the allosteric transition machinery and (b) a specific com-

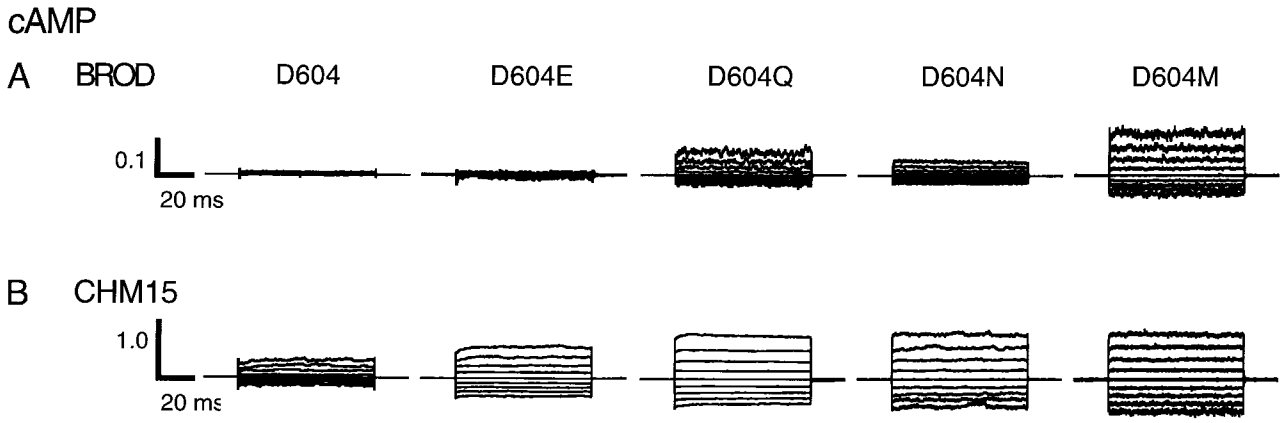

FIGURE 4. Current families for wild-type and mutant channels activated by cAMP. Current families are shown from inside-out patches excised from *Xenopus laevis* oocytes expressing BROD (A) and CHM15 (B) channels with mutations at position 604. Currents were elicited by 16 mM cAMP and voltage pulses from 0 mV to potentials between −80 and +80 mV in 20-mV steps. Leak currents in the absence of cyclic nucleotides were subtracted. The currents were normalized (using the +80-mV trace) to the maximum current obtained after Ni^{2+} potentiation (Gordon and Zagotta, 1995a) in the presence of a saturating concentration of the best agonist.

ponent due to direct effects on the interaction of the ligand with D604. As can be seen in Fig. 5 A, the $\Delta\Delta G$s for both of the horizontal arrows are negative, indicating that the olfactory amino terminal region makes the allosteric transition more favorable for both cGMP and cAMP. The difference between the values of the two $\Delta\Delta G$s should subtract out the nonspecific effect while leaving the direct effects. This difference is referred to as the coupling energy. Since CNG channels have four subunits (Liu et al., 1996; Varnum and Zagotta, 1996), the coupling energies reflect the sum of the direct interactions occurring in each subunit. For this cycle, the coupling energy was only 0.49 kcal/mol, indicating that the effect of substituting the amino terminal region is relatively cyclic nucleotide independent. This result was an expected finding since it has been previously shown that the effect of the olfactory amino terminal region is cyclic nucleotide independent (Liu et al., 1994; Goulding et al., 1994; Gordon and Zagotta, 1995b). Thus, the differences in the way cAMP and cGMP interact with the channel because of the differences in their purine ring structures are preserved on substituting the olfactory amino terminal region. That the effect of the olfactory amino terminal region was cyclic nucleotide independent was also reflected in the macroscopic traces; the trends across the D604 mutants were similar in both the CHM15 and BROD backgrounds.

Illustrated in Fig. 5 B is a thermodynamic mutant cycle analysis of the interaction between D604 and the cyclic nucleotide. Here the D604M mutation makes cGMP a worse agonist ($\Delta\Delta G$ = 4.09 kcal/mol), but makes cAMP a better agonist ($\Delta\Delta G$ = −1.79 kcal/mol). Equivalently, the cyclic nucleotide selectivity was inverted by the D604M mutation, as evidenced by the negative value for $\Delta\Delta G$ ($\Delta\Delta G$ = −1.00 kcal/mol) between cGMP and cAMP on D604M and positive value for $\Delta\Delta G$ ($\Delta\Delta G$ = 4.88 kcal/mol) between cGMP and cAMP on D604. Here, the coupling energy was large and negative (coupling energy = −5.88 kcal/mol), indicating a high degree of interaction between the amino acid at position 604 and the purine ring of the cyclic nucleotide.

Summarized in Table I are the coupling energies for each of the possible thermodynamic mutant cycle comparisons for the 10 different mutants with the three different cyclic nucleotides. All energies of magnitude ≥2.5 kcal/mol are double underlined, and all energies of magnitude between 2 and 2.5 kcal/mol are single underlined. As seen along the diagonal, the coupling energies of changes in the amino terminal region with changes in cyclic nucleotide were generally small. We interpret this to mean that the effect of the olfactory amino terminal region was cyclic nucleotide independent. Note that the coupling energies between CHM15 and BROD were slightly larger than for the other comparisons, probably because the fractional activations of cGMP and cIMP on CHM15 were so large that the method of using Ni^{2+} potentiation to measure ΔG^0 loses resolution. In addition, all of the cells comparing the BROD-D604M and CHM15-D604M to the BROD, CHM15, BROD-D604E, and CHM15-D604E between cIMP and cAMP and between cGMP and cAMP are underlined. This result strongly indicates that cAMP is sensing the amino acid at position 604 quite differently from cIMP and cGMP. This result gives good support for the hypothesis proposed by Varnum et al. (1995) that an acidic residue at position 604 in BROD channels is critical for ligand discrimination and interacts directly with the purine ring of the cyclic nucleotide (Fig. 1). This conclusion is also supported by the fact

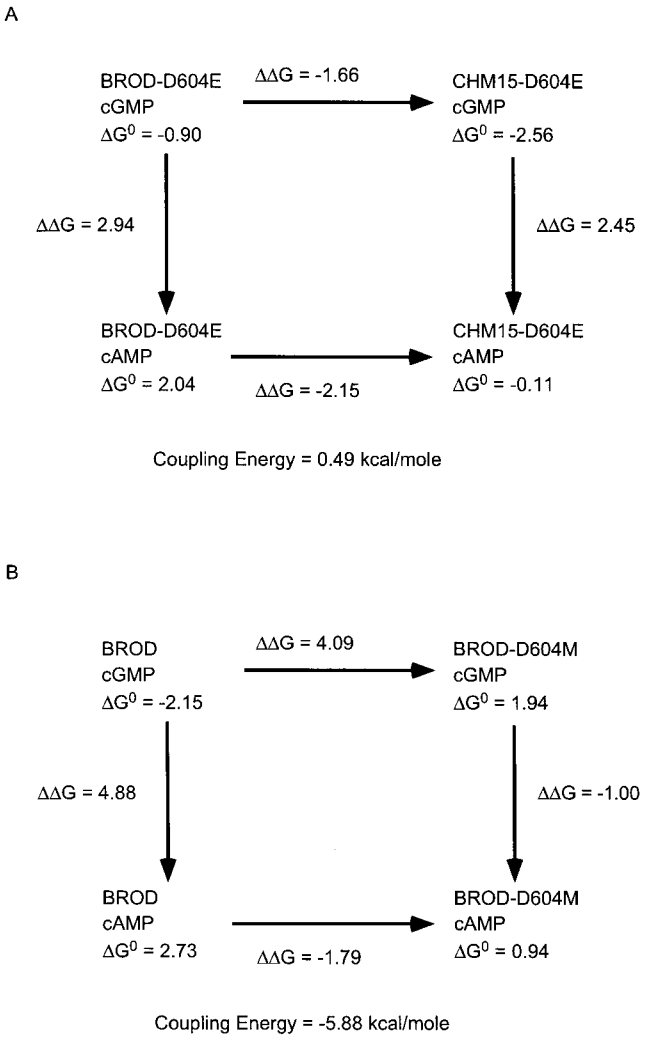

FIGURE 5. Thermodynamic mutant cycles identify direct interactions between cyclic nucleotides and D604. (A) The effect of substituting the olfactory amino terminal region for the BROD amino terminal region was cyclic nucleotide independent. (B) The effect of mutating D604 to D604M was strongly cyclic nucleotide dependent, indicating that the amino acid at position 604 is critical for cGMP vs. cAMP discrimination by the channel.

that the majority of the cells for the more conservative D604Q and D604N vs. D604 and D604E in the BROD and CHM15 backgrounds were also >2 kcal/mol for cIMP vs. cAMP and cAMP vs. cGMP.

For the cGMP vs. cIMP comparisons, the coupling energies were smaller in magnitude, as expected since the chemical differences between cGMP and cIMP are smaller relative to their differences with cAMP. As can be seen in Table I, there was a ≥2 kcal/mol coupling energy in the BROD vs. BROD-D604N, CHM15-D604N, BROD-D604M, and CHM15-D604M. Since the only difference between cGMP and cIMP is at the 2-positions of their purine rings, this finding supports the hypothesis of Varnum et al. (1995) that the guanine 2-amino group of cGMP interacts with D604 (Fig. 1). For CHM15, the same analysis did not reveal large coupling energies with the same four constructs vs. CHM15. However, we do not feel that this negative result indicates a lack of interaction. Rather, it is probable that we were not able to pick up a differential interaction because the CHM15 construct had such a favorable ΔG^0 for the allosteric transition so that the currents were nearly maximal without Ni^{2+} in the presence of cGMP and cIMP. For BROD-D604E and CHM15-D604E, the coupling energies with BROD-D604M and CHM15-D604M ranged from −0.92 to −1.46 kcal/mol. These values are smaller than the values of −2.21 and −2.30 kcal/mol between BROD and BROD-D604M and CHM15-D604M, possibly reflecting weaker interactions because of the larger side chain of glutamate over aspartate. Thus, overall, we conclude that the comparisons between the D604 and D604E constructs and the D604M constructs provide support for the hypothesis of Varnum et al. (1995) that cIMP forms one hydrogen bond with D604 while cGMP forms two. The coupling energies we measured are within the range of energies expected for such an interaction (Fersht et al., 1985).

Effects of Position 604 Mutations Are on Gating, not Single-Channel Amplitude

To probe the effects on the opening and closing rate constants, not just the overall ΔG^0, we obtained single-channel recordings at +80 mV for each of the 10 constructs in the presence of saturating concentrations of cGMP, cIMP, and cAMP. From each recording, we selected regions where a single channel was active, and we omitted from our analysis quiescent periods 200 ms or longer in duration (Sunderman and Zagotta, 1999). Representative 200-ms portions of our recordings are illustrated in Figs. 6, 8, and 10 for cGMP, cIMP, and cAMP, respectively. The amplitude histograms for the recordings shown in Figs. 6, 8, and 10 are shown in Figs. 7, 9, and 11.

Fig. 6 shows representative single-channel traces for the 10 constructs activated by 16 mM cGMP. As 16 mM cGMP is a saturating concentration, the kinetics that we observe do not reflect the rate constants of binding or unbinding of cGMP. Rather, they reflect transitions after the full complement of ligands has bound to the channel. For D604, the channel was highly activated in the BROD construct, but more so for CHM15. In both cases, the single-channel conductance was the same. We compare the open probabilities and single-channel current level in the amplitude distributions in Fig. 7, which shows BROD and CHM15 distributions side-by-side. As expected given the slightly lower fractional activation of D604E compared with D604 in macroscopic experiments, the open probability of D604E was slightly lower than for D604. For BROD-D604Q and BROD-D604N, the open probability decreased substan-

t a b l e i

Summary of Coupling Energies

BROD			CHM15			BROD-D604E			CHM15-D604E			BROD-D604Q			CHM15-D604Q			BROD-D604N			CHM15-D604N			BROD-D604M			CHM15-D604M			
G–I	I–A	A–G	G–I	I–A	A–G	G–I	I–A	A–G	G–I	I–A	A–G	G–I	I–A	A–G	G–I	I–A	A–G	G–I	I–A	A–G	G–I	I–A	A–G	G–I	I–A	A–G	G–I	I–A	A–G	
0			−1.80			−0.84			−1.29			−1.35			−1.29			−2.05			−2.07			−2.21			−2.30			G–I BROD
	0			0.15			−1.10			−1.13			−3.12			−2.92			−2.60			−2.40			−3.73			−3.73		I–A
		0			1.65			1.94			2.43			4.47			4.21			4.65			4.46			5.88			6.03	A–G
			0			0.96			0.51			0.45			0.51			−0.25			−0.27			−0.41			−0.50			G–I CHM15
				0			−1.25			−1.28			−3.27			−3.07			−2.75			−2.54			−3.82			−3.88		I–A
					0			0.29			0.78			2.82			2.56			2.99			2.81			4.23			4.38	A–G
						0			−0.45			−0.51			−0.45			−1.21			−1.23			−1.37			−1.46			G–I BROD-D604E
							0			−0.03			−2.02			−1.82			−1.50			−1.30			−2.57			−2.63		I–A
								0			0.49			2.53			2.27			2.71			2.52			3.94			4.09	A–G
									0			−0.06			0.00			−0.75			−0.77			−0.92			−1.01			G–I CHM15-D604E
										0			−1.99			−1.79			−1.46			−1.26			−2.54			−2.59		I–A
											0			2.05			1.78			2.22			2.03			3.45			3.60	A–G
												0			0.06			−0.70			−0.72			−0.86			−0.95			G–I BROD-D604Q
													0			0.20			0.53			0.73			−0.55			−0.60		I–A
														0			−0.26			0.17			−0.01			1.41			1.55	A–G
															0			−0.75			−0.77			−0.92			−1.01			G–I CHM15-D604Q
																0			0.32			0.52			−0.75			−0.81		I–A
																	0			0.43			0.25			1.67			1.81	A–G
																		0			−0.02			−0.16			−0.25			G–I BROD-D604N
																			0			0.20			−1.07			−1.13		I–A
																				0			−0.18			1.24			1.38	A–G
																					0			−0.14			−0.23			G–I CHM15-D604N
																						0			−1.27			−1.33		I–A
																							0			1.42			1.56	A–G
																								0			−0.09			G–I BROD-D604M
																									0			−0.06		I–A
																										0			0.15	A–G
																											0			G–I CHM15-D604M
																												0		I–A
																													0	A–G

Coupling energies for each thermodynamic mutant cycle comparison are tabulated as shown. G–I indicates the coupling energy between cGMP and cIMP, I–A indicates the coupling energy between cIMP and cAMP, and A–G indicates the coupling energy between cAMP and cGMP. The cells that indicate the effect of the olfactory amino terminus on cyclic nucleotide selectivity for each amino acid at position 604 are shown on the diagonal. Cells with coupling energies with an absolute value between 2 and 2.5 kcal/mol are underlined. Cells with coupling energies with an absolute value exceeding 2.5 kcal/mol are double underlined.

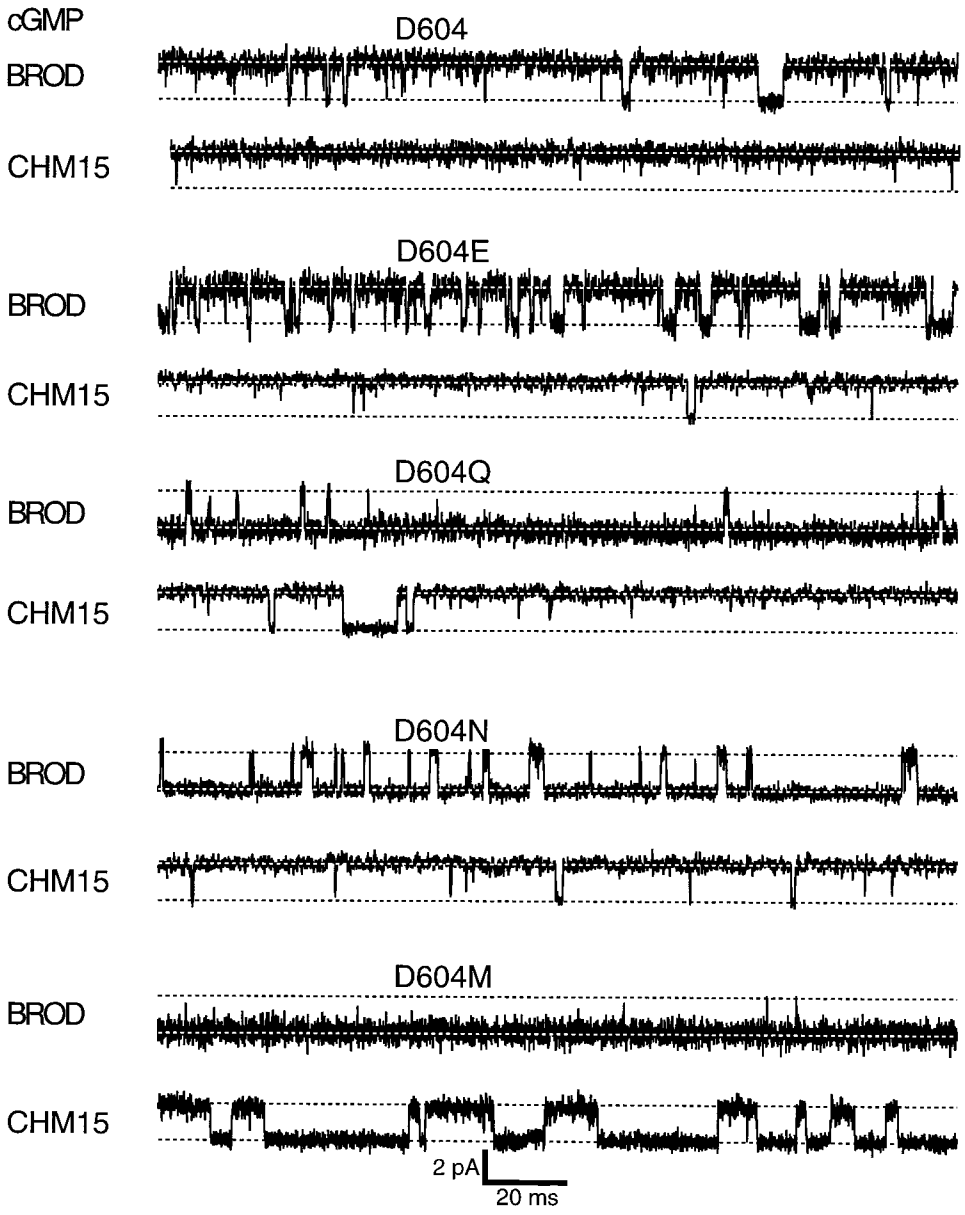

FIGURE 6. Representative single-channel traces at a saturating concentration of cGMP. Single-channel currents for all 10 constructs were recorded in the presence of 16 mM cGMP with the membrane voltage clamped at +80 mV. The upper and lower dotted lines indicated the open and closed levels, respectively, and are separated by 2.3 pA.

tially. For BROD-D604M, the open probability was very low but increased to ~0.5 in CHM15-D604M. In each case, the single-channel conductance appears to be unaffected by mutations at position 604 or the presence of the olfactory amino terminal region, and openings appear to be to only the full amplitude level, not to subconductance states. Thus, the large differences in fractional activation determined from the macroscopic current experiments are due entirely to differences in the open probabilities produced by D604 mutations and the olfactory amino terminal region. In particular, the open probabilities in cGMP decreased as D604 became less polar and increased with the addition of the olfactory amino terminal region.

For cIMP activation of the 10 constructs, representative traces and amplitude histograms are shown in Figs. 8 and 9, respectively. Here, the trend across the constructs was quite similar to the trend for cGMP, although there were a few differences. With cIMP, the open probability was only 74% in D604. Like for cGMP, the open probability decreased as the amino acid at position 604 became less polar and increased with the addition of the olfactory amino terminal region. Interestingly, openings in BROD-D604M were slightly more numerous and longer-lived than for cGMP.

For cAMP activation across the 10 constructs, representative traces and amplitude histograms are shown in Figs. 10 and 11. As can be seen here, the open probability was low when a polar residue was present at position 604. For BROD-D604M, the openings were significantly longer in duration. The same trends were observed in the CHM15 constructs.

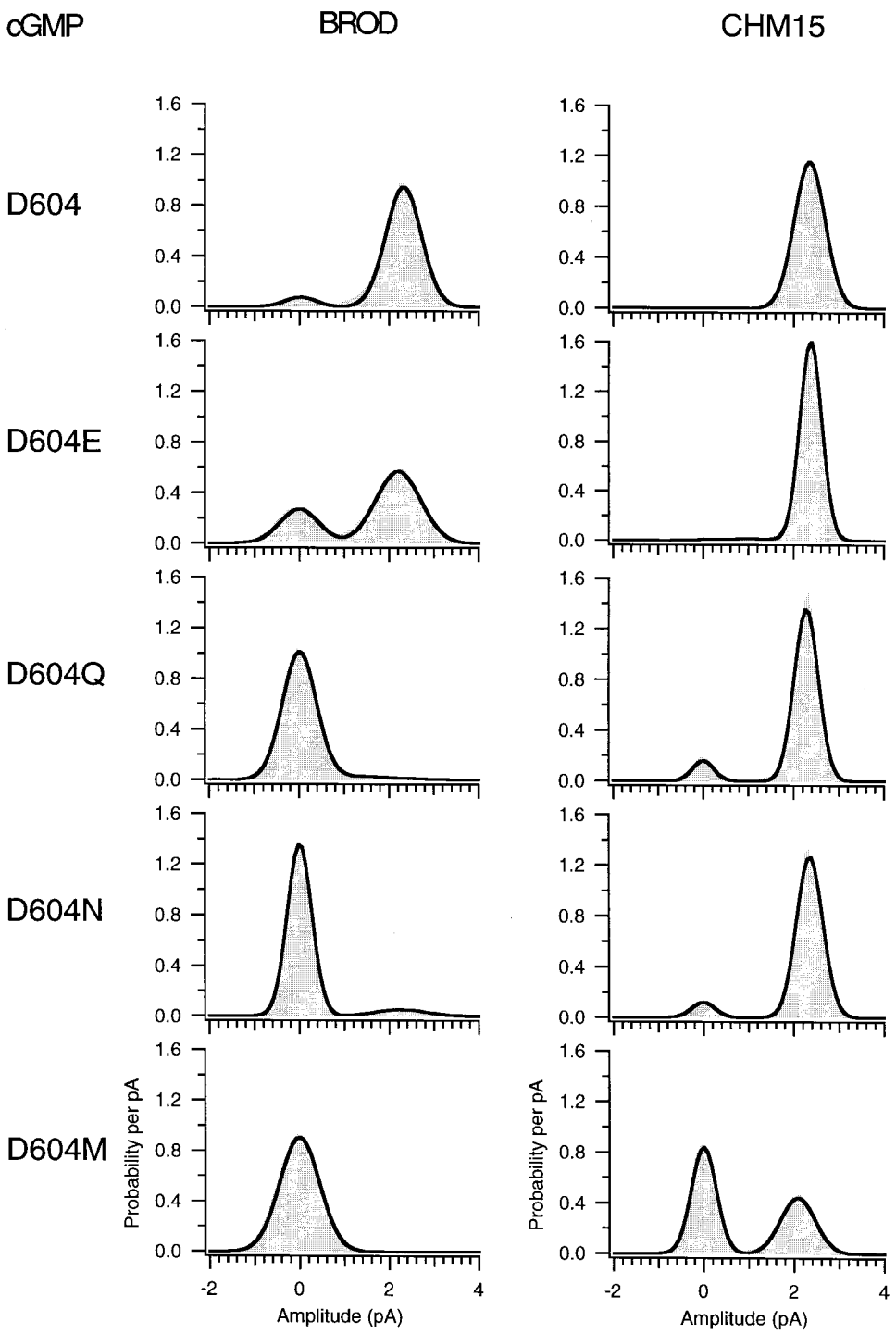

FIGURE 7. Amplitude histograms for activation by a saturating concentration of cGMP. Amplitude histograms corresponding to the representative traces in Fig. 6 are shown. The histograms were fit to the sum of two Gaussians, and the peak of the closed level Gaussian was used to subtract off leak currents. The parameters for the amplitude histograms were as follows: for BROD, σ_{closed} = 480 fA, σ_{open} = 560 fA, P_{open} = 0.95; for CHM15, σ_{closed} = 1.6 pA, σ_{open} = 340 fA, P_{open} = 0.99; for BROD-D604E, σ_{closed} = 490 fA, σ_{open} = 430 fA, P_{open} = 0.71; for CHM15-D604E, σ_{closed} = 850 fA, σ_{open} = 240 fA, P_{open} = 0.97; for BROD-D604Q, σ_{closed} = 380 fA, σ_{open} = 890 fA, P_{open} = 0.06; for CHM15-D604Q, σ_{closed} = 240 fA, σ_{open} = 270 fA, P_{open} = 0.91; for BROD-D604N, σ_{closed} = 270 fA, σ_{open} = 560 fA, P_{open} = 0.07; for CHM15-D604N, σ_{closed} = 260 fA, σ_{open} = 290 fA, P_{open} = 0.92; for BROD-D604M, σ_{closed} = 440 fA, σ_{open} = 1.33 pA, P_{open} = 0.003; for CHM15-D604M, σ_{closed} = 270 fA, σ_{open} = 390 fA, P_{open} = 0.42.

Hidden Markov Model Analysis of Single-Channel Patch-Clamp Recordings

We analyzed the single-channel kinetics for each of the 10 constructs using a hidden Markov modeling (HMM) approach. The HMM approach, described in detail in the accompanying paper (Sunderman and Zagotta, 1999), directly estimates the rate constants for a given specified kinetic scheme and uses iterative techniques to converge on the maximum likelihood set of rate constants. The HMM approach provides a maximum likelihood value that allows the number of closed and open states required to explain the data to be determined. In the previous paper, we found that a simple two-state C ↔ O scheme is not sufficient to explain the kinetics at saturating ligand concentrations. Rather, an additional closed state was required. Adding this addi-

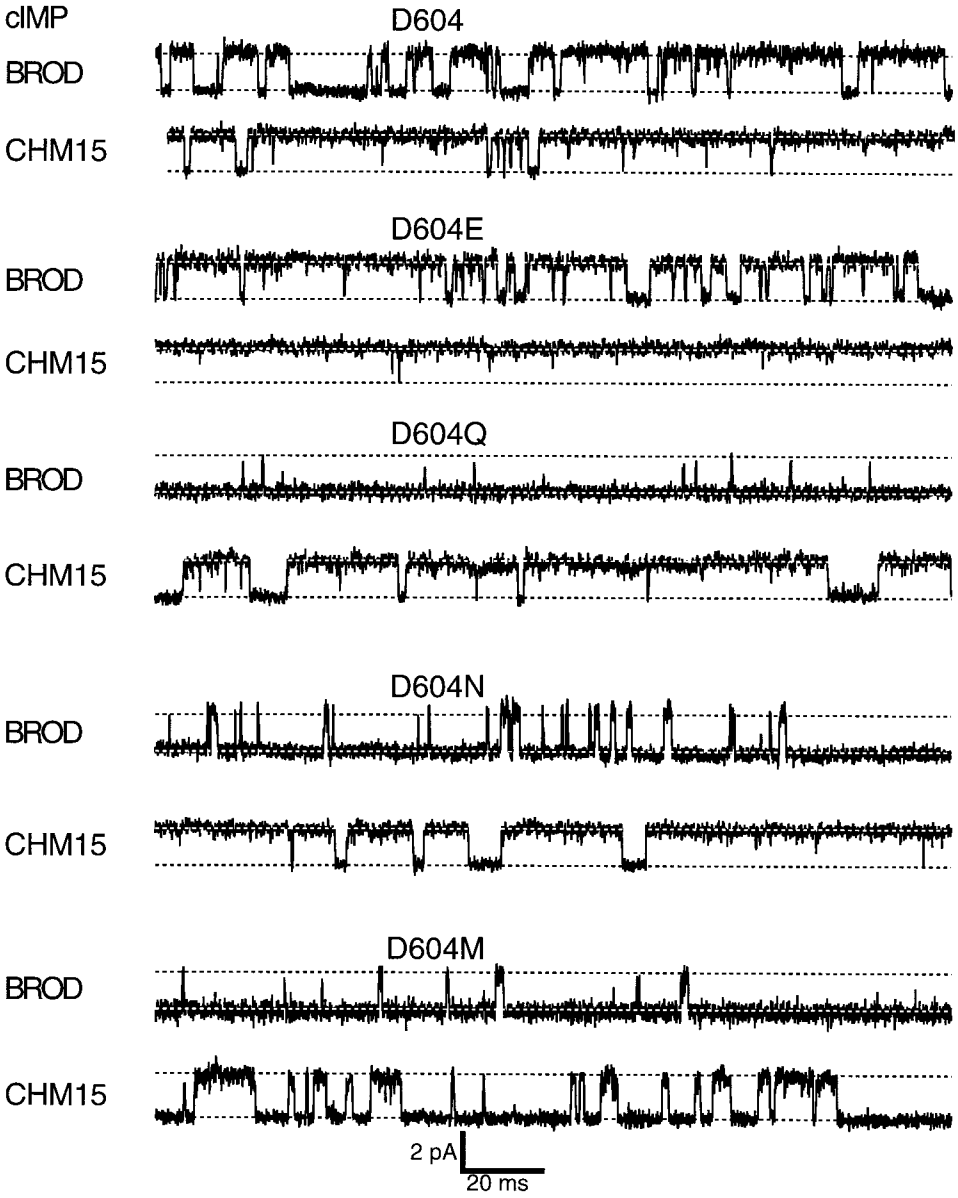

FIGURE 8. Representative single-channel traces at a saturating concentration of cIMP. Single-channel currents for all 10 constructs were recorded in the presence of 16 mM cIMP with the membrane voltage clamped at +80 mV. The upper and lower dotted lines indicated the open and closed levels, respectively, and are separated by 2.3 pA.

tional closed state outside the activation pathway (as in $C_0 \leftrightarrow O_1 \leftrightarrow C_2$) or within the activation pathway (as in $C_{0'} \leftrightarrow C_{1'} \leftrightarrow O_{2'}$) significantly improved the description of the kinetics at saturating ligand concentrations. Since the likelihoods for the $C_0 \leftrightarrow O_1 \leftrightarrow C_2$ and $C_{0'} \leftrightarrow C_{1'} \leftrightarrow O_{2'}$ linear schemes are identical, we could not discriminate between these two schemes. However, we prefer the $C_0 \leftrightarrow O_1 \leftrightarrow C_2$ scheme because there was cyclic nucleotide dependence in only the first transition of the $C_0 \leftrightarrow O_1 \leftrightarrow C_2$ scheme. Also, the $C_0 \leftrightarrow O_1 \leftrightarrow C_2$ scheme has the simple physical interpretation of the first transition being the allosteric transition and the second transition being to a flicker closed state out of the activation pathway. While the underlying mechanism is undoubtedly more complex than two closed and one open states, this mechanism adequately describes our data and provides a physical interpretation of the results. The qualitative conclusions concerning the effects of mutations on the stability of the open state and transition state should still be valid for a $C_{0'} \leftrightarrow C_{1'} \leftrightarrow O_{2'}$ scheme and more complex models. These conclusions are based on effects of these mutations on the open and closed durations and are not dependent on any particular model.

For the analysis of the 10 constructs described in this paper, we determined the rate constants for the $C_0 \leftrightarrow O_1 \leftrightarrow C_2$ scheme. Shown in Fig. 12 is a summary of the rate constants from multiple patches for the $C_0 \leftrightarrow O_1$ step for all 10 constructs and for all three cyclic nucleotides. The opening rate k_{01} became progressively slower for cGMP as the amino acid at position 604 became less polar (Fig. 12 A). This effect was observed in

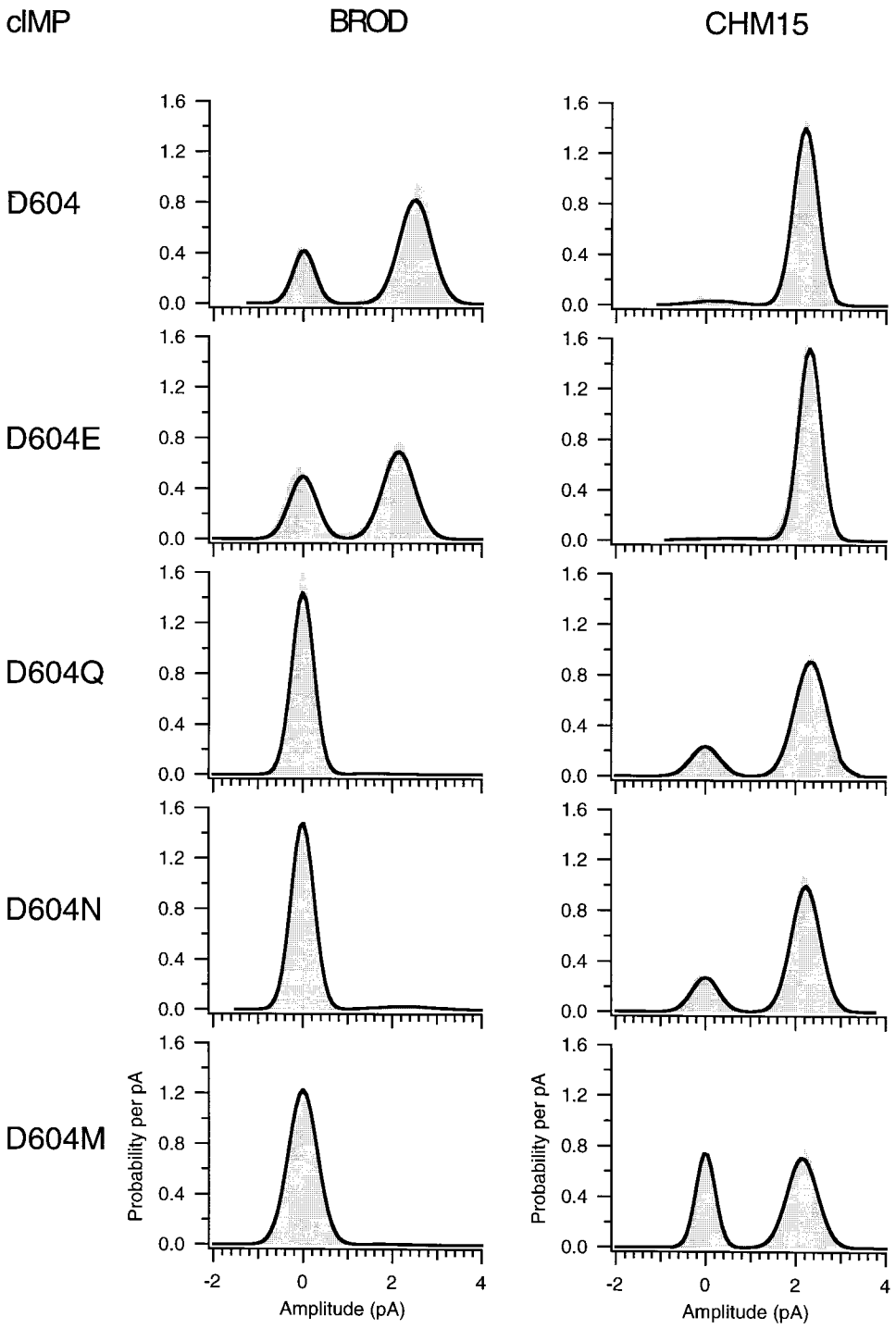

FIGURE 9. Amplitude histograms for activation by a saturating concentration of cIMP. Amplitude histograms corresponding to the representative traces in Fig. 8 are shown. The histograms were fit to the sum of two Gaussians, and the peak of the closed level Gaussian was used to subtract off leak currents. The parameters for the amplitude histograms were as follows: for BROD, σ_{closed} = 240 fA, σ_{open} = 360 fA, P_{open} = 0.74; for CHM15, σ_{closed} = 530 fA, σ_{open} = 270 fA, P_{open} = 0.96; for BROD-D604E, σ_{closed} = 300 fA, σ_{open} = 360 fA, P_{open} = 0.62; for CHM15-D604E, σ_{closed} = 930 fA, σ_{open} = 250 fA, P_{open} = 0.96; for BROD-D604Q, σ_{closed} = 250 fA, σ_{open} = 610 fA, P_{open} = 0.011; for CHM15-D604Q, σ_{closed} = 320 fA, σ_{open} = 360 fA, P_{open} = 0.81; for BROD-D604N, σ_{closed} = 260 fA, σ_{open} = 650 fA, P_{open} = 0.044; for CHM15-D604N, σ_{closed} = 290 fA, σ_{open} = 320 fA, P_{open} = 0.80; for BROD-D604M, σ_{closed} = 320 fA, σ_{open} = 610 fA, P_{open} = 0.009; for CHM15-D604M, σ_{closed} = 210 fA, σ_{open} = 340 fA, P_{open} = 0.59.

both the BROD and CHM15 constructs. For cIMP, the slowing of the k_{01} rate was smaller but in the same direction. For cAMP, the k_{01} rate constant was nearly independent of construct, perhaps increasing slightly. In Fig. 12 B, we see that the effects of the D604 mutations on the k_{10} rate constant are larger than for the k_{01} rate constant. For cGMP, there was a progressive speeding up of the closing rate (k_{10}) constant as the amino acid at position 604 became less polar. For cIMP, the trend across constructs was generally the same but smaller in magnitude. For cAMP, the k_{10} rate constant was relatively independent of the amino acid at position 604, thus indicating that the interactions of cAMP with D604 are unimportant for determining the closing rate constant.

For the CHM15 constructs, the effect on the k_{10} rate constant was remarkable. For each mutation at position 604 in the BROD construct, the corresponding muta-

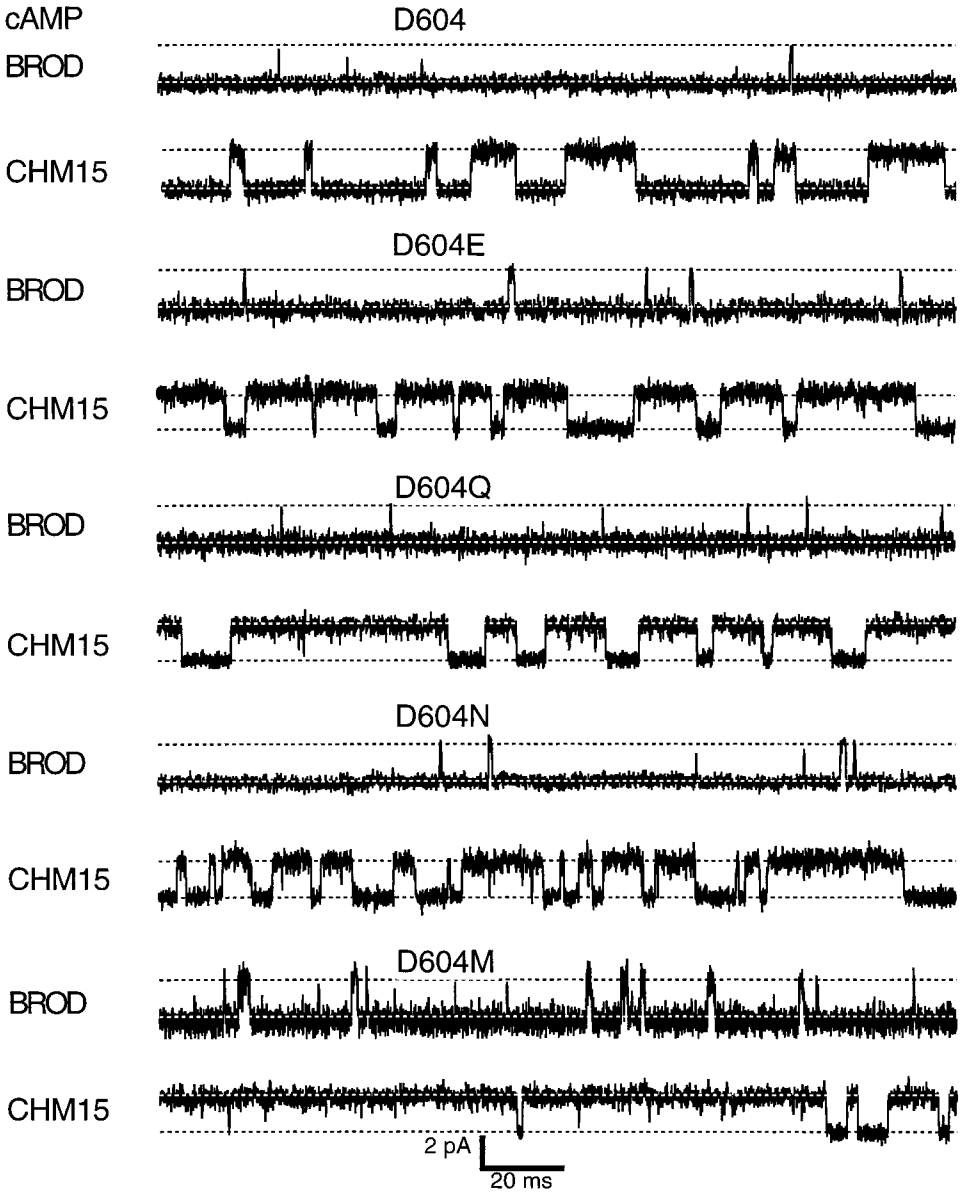

FIGURE 10. Representative single-channel traces at a saturating concentration of cAMP. Single-channel currents for all 10 constructs were recorded in the presence of 16 mM cAMP with the membrane voltage clamped at +80 mV. The upper and lower dotted lines indicated the open and closed levels, respectively, and are separated by 2.3 pA.

tion in the CHM15 construct was ~20–100-fold slower. This result contrasts with the result for the opening rate constant, which appeared to be relatively independent of the presence or absence of the olfactory amino terminal region. The large effect on the closing rate constant indicates that the positive interactions incurred with the substitution of the olfactory amino terminal region are a major determinant of the closing rate constant.

Shown in Fig. 13 are the rate constants for the second transition $O_1 \leftrightarrow C_2$ across constructs and for the three cyclic nucleotides. As can be seen in this figure, the reopening rate constant k_{21} was generally independent of cyclic nucleotide and construct and was fast (~5,000/s). The closing rate k_{12} was also generally independent of cyclic nucleotide and construct but was much slower (~100/s). Thus, the equilibrium for the $O_1 \leftrightarrow C_2$ step is strongly toward the open state, and sojourns in the C_2 state were short in duration, not unlike what would be expected for flickery open-channel block. More importantly, the effects of the D604 mutations and the olfactory amino terminal region are selective for the first transition of $C_0 \leftrightarrow O_1 \leftrightarrow C_2$, as was previously shown for the effects of cyclic nucleotides and Ni^{2+} (Sunderman and Zagotta, 1999). The observation that each of these modifications is affecting the same step provides further support for the hypothesis that the first transition of the $C_0 \leftrightarrow O_1 \leftrightarrow C_2$ scheme is the allosteric transition, and the second transition is not involved in the allosteric transition.

Correspondence between Macroscopic and Single-Channel Current Recordings

A comparison between the values for ΔG^0 calculated as $-RT \ln(k_{01}/k_{10})$ from the single-channel experiments,

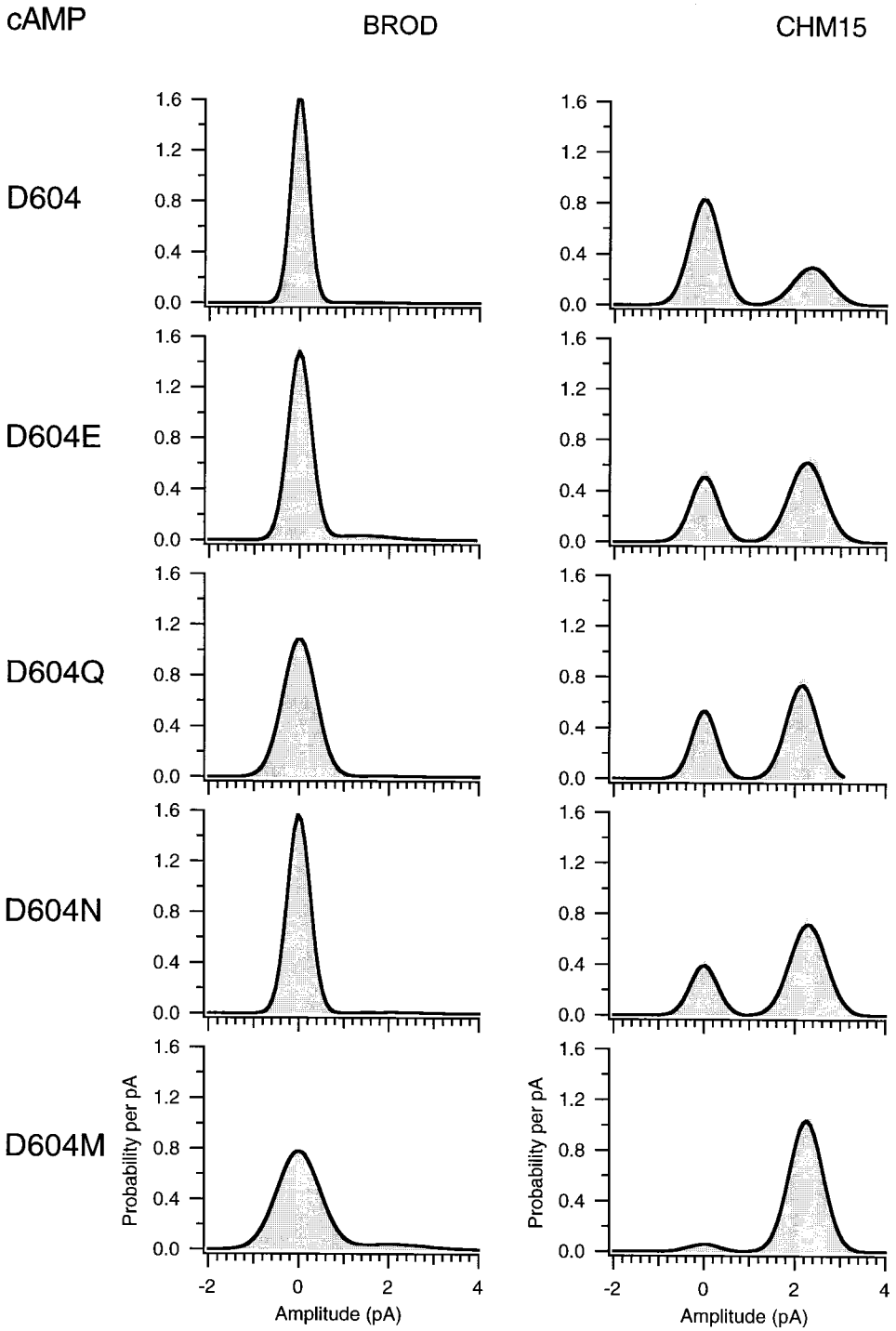

FIGURE 11. Amplitude histograms for activation by a saturating concentration of cAMP. Amplitude histograms corresponding to the representative traces in Fig. 10 are shown. The histograms were fit to the sum of two Gaussians, and the peak of the closed level Gaussian was used to subtract off leak currents. The parameters for the amplitude histograms were as follows: for BROD, σ_{closed} = 290 fA, σ_{open} = 780 fA, P_{open} = 0.004; for CHM15, σ_{closed} = 330 fA, σ_{open} = 410 fA, P_{open} = 0.31; for BROD-D604E, σ_{closed} = 230 fA, σ_{open} = 630 fA, P_{open} = 0.05; for CHM15-D604E, σ_{closed} = 300 fA, σ_{open} = 390 fA, P_{open} = 0.61; for BROD-D604Q, σ_{closed} = 360 fA, σ_{open} = 580 fA, P_{open} = 0.009; for CHM15-D604Q, σ_{closed} = 270 fA, σ_{open} = 340 fA, P_{open} = 0.62; for BROD-D604N, σ_{closed} = 250 fA, σ_{open} = 660 fA, P_{open} = 0.015; for CHM15-D604N, σ_{closed} = 300 fA, σ_{open} = 390 fA, P_{open} = 0.71; for BROD-D604M, σ_{closed} = 470 fA, σ_{open} = 770 fA, P_{open} = 0.082; for CHM15-D604M, σ_{closed} = 330 fA, σ_{open} = 370 fA, P_{open} = 0.95.

relative to the values for $\Delta G^0 = -RT \ln L$, where L is the equilibrium constant for the allosteric transition and was determined using Ni^{2+} potentiation of macroscopic experiments, is shown in Fig. 14 (see MATERIALS AND METHODS). Overall, the correspondence between the values is good. It may be noted that for BROD D604Q, D604N, and D604M, the median single-channel estimate for ΔG^0 was slightly larger than the macroscopic estimate in each case. The probable explanation for this observation is that currents obtained with Ni^{2+} in macroscopic experiments slightly underestimate the maximum current. This underestimation is occurring because the ΔG^0 for the transition is so unfavorable for each of these constructs that, even with Ni^{2+}, the currents do not approximate the theoretical maximum current that would be obtained if the fractional activation were 1. Note that this slight difference could not be explained by error in the determination of the number of channels in a single-channel

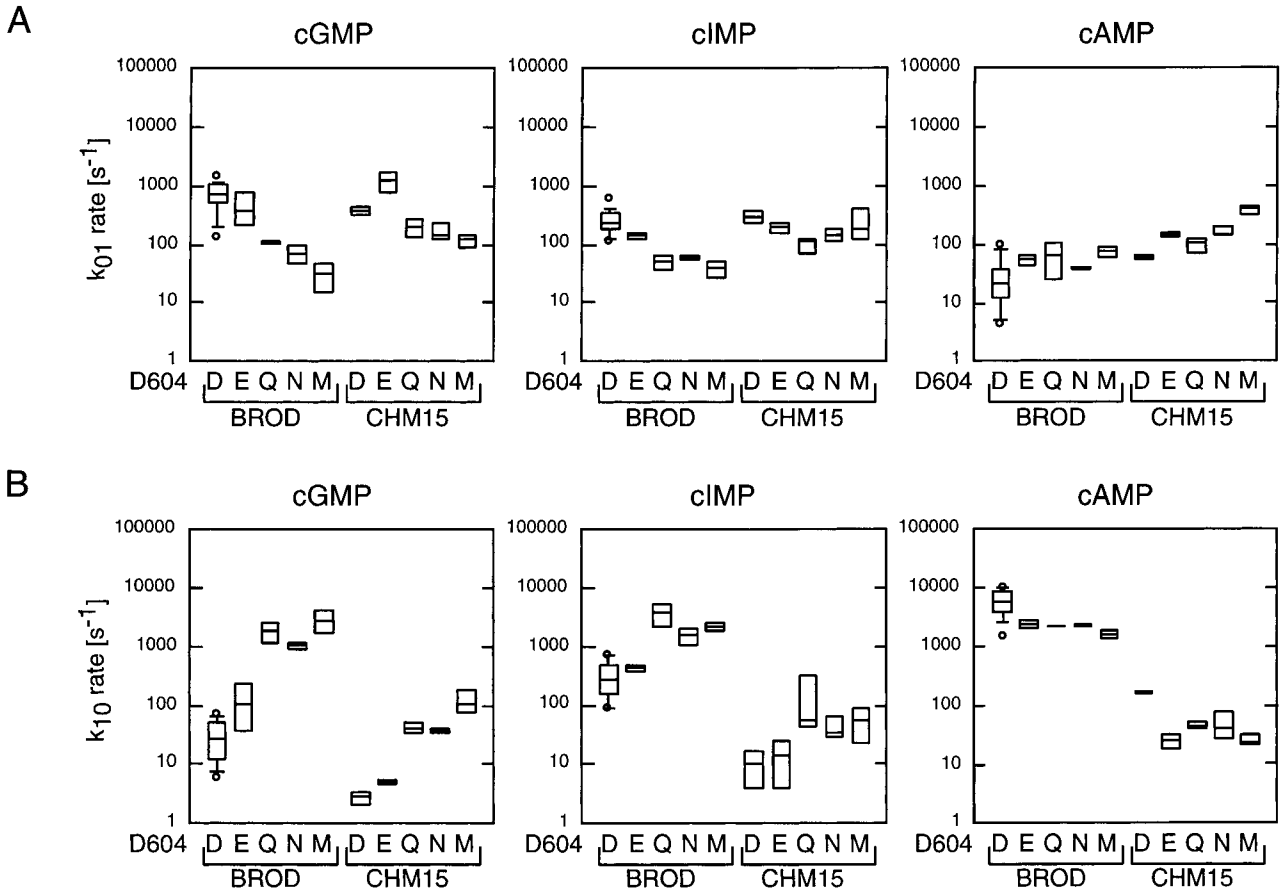

FIGURE 12. Box plot summaries for k_{01} and k_{10}. Box plots of the k_{01} (A) and k_{10} (B) rate constants for the $C_0 \leftrightarrow O_1 \leftrightarrow C_2$ scheme are shown for all 10 constructs for cGMP, cIMP, and cAMP. Values for the rate constants were determined by HMM analysis. The horizontal line within each box indicates the median of the data; boxes show the 25th and 75th percentiles of the data; whiskers show the 5th and 95th percentiles. Extreme data points are also indicated.

patch, as the effect of having too many channels would be to increase the opening rate constant, thus making the ΔG^0 more favorable, not less. This figure illustrates that there was generally good correspondence between the values obtained for the macroscopic and single-channel experiments. This result supports the use of Ni^{2+} for the estimation of ΔG^0 from macroscopic experiments and provides additional evidence that the $C_0 \leftrightarrow O_1$ transition represents the transition modulated by Ni^{2+}.

Effects of Allosteric Modulation on the Free Energy Profiles for the Allosteric Transition

Using Eyring rate theory (Eyring, 1935), we converted the median rate constants we obtained from our HMM computations to activation energies (see MATERIALS AND METHODS). Eyring rate theory assumes that there is a quasi-equilibrium between a high energy transition state and the ground state, and that the rate of break down to product of the high energy intermediate depends on the vibrational energy of a covalent bond at room temperature. Other theories have been proposed to explain the slow rate of protein conformational changes (Jackson, 1993); however, Eyring rate theory is generally accepted and provides a unique estimate of the transition state energies (Creighton, 1993). While the absolute activation energy ($\Delta G^{\ddagger}$) is dependent on estimates of a preexponential factor, the changes in activation energy ($\Delta\Delta G^{\ddagger}$) are less dependent on this estimate.

Fig. 15 A illustrates the energetics for the allosteric transition for the three cyclic nucleotides. In this figure, the energy profiles were aligned at 0 kcal/mol when the channels were in the closed state (C_0). As can be seen in this figure, the overall ΔG^0 for the allosteric transition is between -2 and 3 kcal/mol for cGMP and cAMP, respectively. Since these cyclic nucleotides differ in only the most distal portion of their purine ring, we conclude that the cyclic nucleotide–binding domain interacts with the purine ring of the cyclic nucleotides differently during the allosteric transition. The energetics for these favorable cyclic nucleotide–binding domain interactions must therefore be determinants of the stability of the open state. Since the energy of the transition state ($\Delta G^{\ddagger}$) also differs among the cyclic nu-

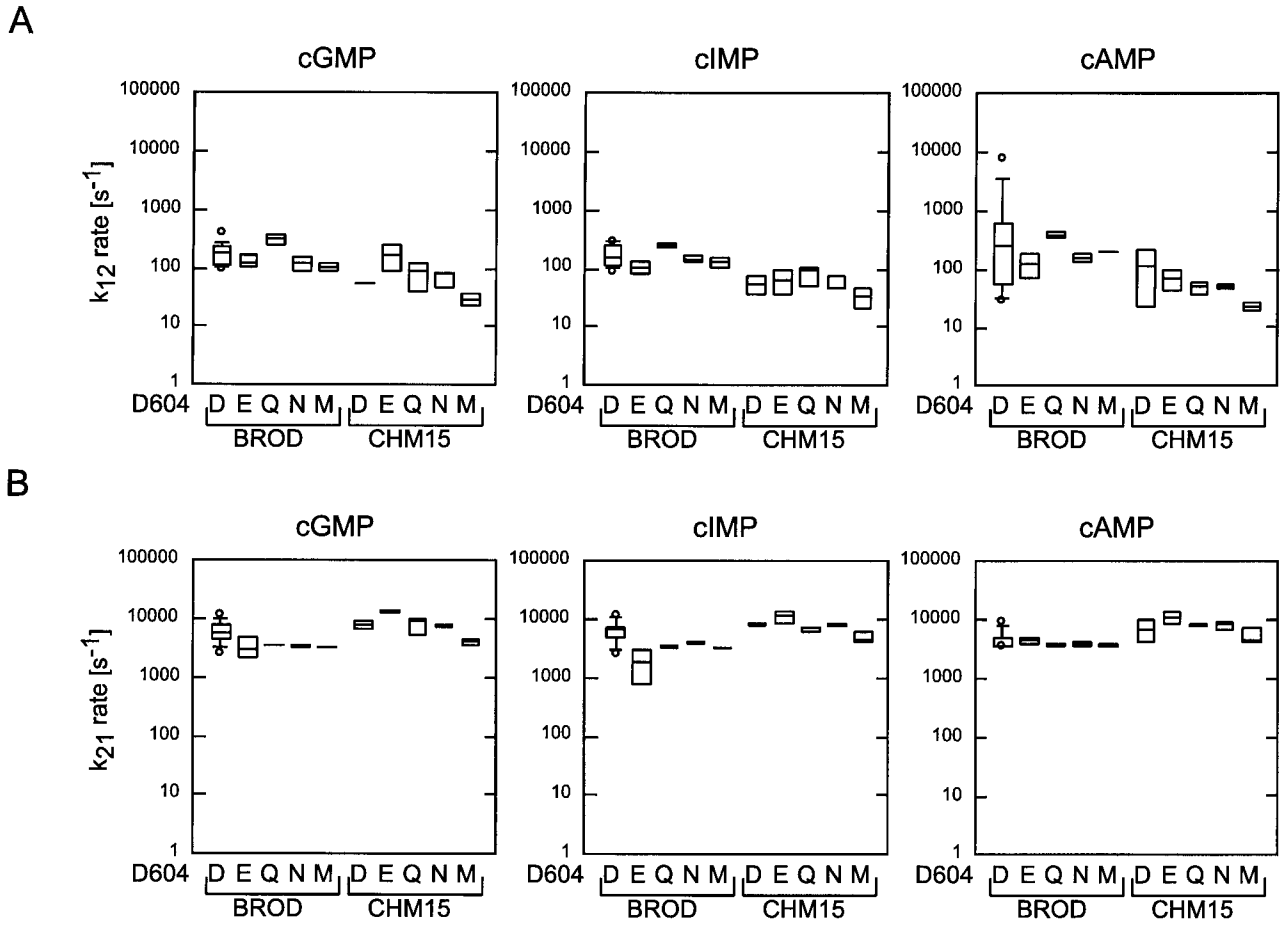

FIGURE 13. Box plot summaries for k_{12} and k_{21}. Box plots of the k_{12} (A) and k_{21} (B) rate constants for the $C_0 \leftrightarrow O_1 \leftrightarrow C_2$ scheme are shown for all 10 constructs for cGMP, cIMP, and cAMP. Values for the rate constants were determined by HMM analysis.

cleotides, we conclude that these interactions are partially formed at the time of the transition state and serve to reduce the energetic barrier for activation.

The effects of Ni^{2+} presented in the previous paper (Sunderman and Zagotta, 1999) on the transition-state energies are diagrammed in Fig. 15 B. This figure illustrates that, like the cyclic nucleotides, Ni^{2+} also affects the transition state energy and stability of the open state relative to the closed state. For both cIMP and cAMP, the presence of Ni^{2+} stabilizes the open state and has a small effect on the energy of the transition state. This finding suggests that the movement of the H420 residues on each of the subunits of the channel into the Ni^{2+} coordinating position is associated with channel opening. These interactions between Ni^{2+} and the channel are partially formed at the time of the transition state for the allosteric transition.

Fig. 15 C shows the energetics for activation of BROD and BROD-D604M channels by cGMP. As can be seen in this figure, D604M channels activated by cGMP have an allosteric transition energetically very similar to BROD channels activated by cAMP, both with regard to the standard free energy of the transition and the activation energy. This is a testament to the idea that the purine ring of cGMP interacts directly with D604. Disrupting this interaction with either cAMP or D604 mutations has a very similar effect. Fig. 15 D shows the energetics for activation of BROD and CHM15 channels by cIMP. As can be seen in this figure, the mechanism of action of the olfactory amino terminal region is a stabilization of the open state without affecting the transition state energy. This finding suggests that the stabilizing interactions between the autoexcitatory domain of the olfactory amino terminal region do not form until after the transition state for the allosteric transition. Thus, the interactions of the cyclic nucleotide and the binding site form at the time of the transition state, while the stabilizing effect of the olfactory amino terminal region arises after the transition state.

Fraction of Energetic Effect after the Transition State Reveals the Sequence of Events

To probe the sequence of events underlying the allosteric transition, we calculated the fraction of the energetic effect of the modifications studied that occurs af-

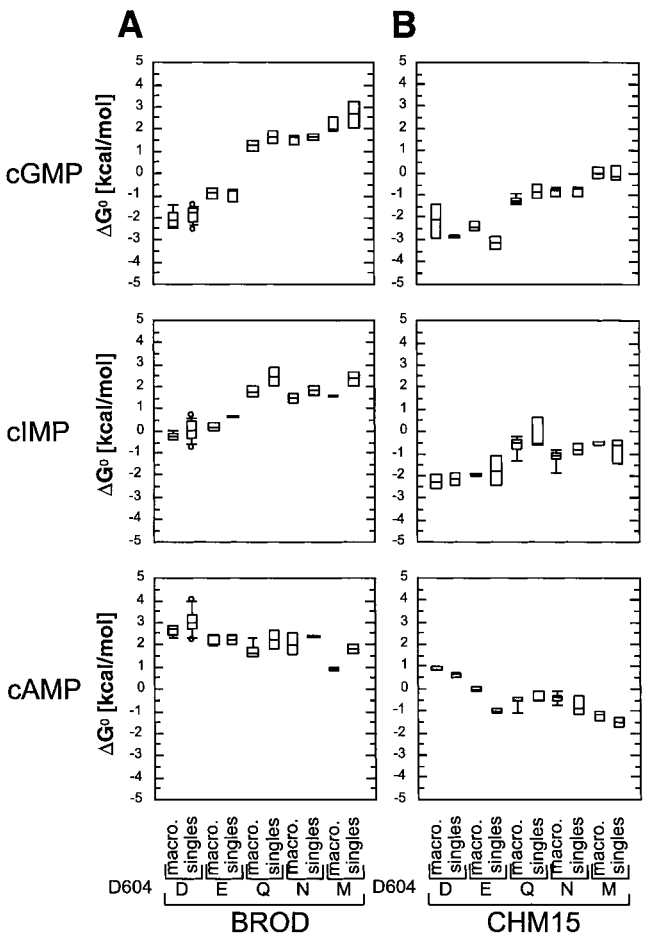

FIGURE 14. Box plot comparison between the values for k_{01}/k_{10} and for L calculated from macroscopic experiments using Ni^{2+} potentiation. Box plots comparing the values for ΔG^0 for the allosteric transition from singles and macroscopic current experiments are shown for the BROD (A) and CHM15 (B) channels.

ter the allosteric transition and plotted the median values in Fig. 16. These calculations were made by considering the effect on the k_{01} and k_{10} rate constants of switching cyclic nucleotide on BROD-D604 channels, switching from D604 to D604M in either the BROD or CHM15 backgrounds and for each of the cyclic nucleotides, applying Ni^{2+} on BROD channels (Sunderman and Zagotta, 1999), and switching from BROD-D604 to CHM15-D604 for each of the cyclic nucleotides. As can be seen in Fig. 16, in each case, the majority of the energetic effect of each modification occurred on the closing rate constant, meaning after the transition state for the allosteric conformational change. Intriguingly, the median fraction of the effect occurring after the transition state was 68% for the interactions of the channel with the portions of the cyclic nucleotides that differ and 70% for the effect of switching to D604M. The close correspondence between these two values gives further support for the hypothesis that the purine rings of the cyclic nucleotides and the amino acid at position 604 interact directly because it indicates that the D604M mutation and switching to a different cyclic nucleotide not only affect both rate constants, but they affect both rate constants commensurately. For Ni^{2+}, there was more variation in the fraction of the energetic effect occurring after the transition state. For the olfactory amino terminal region, the median value was strongly skewed toward the right, indicating that only a small fraction of the energetic effect of the amino terminal region has occurred by the time of the transition state. Hence, we would say that the state-dependent stabilization of the allosteric transition occurs very late in the reaction coordinate. It is tantalizing to conclude that the interactions between the purine ring of the cyclic nucleotide and the amino acid at position 604 occur early in the reaction coordinate. These interactions are followed by the interactions of H420 in the C linker with Ni^{2+}. Finally, the stabilizing interactions with the olfactory amino terminal region, when present, form late in the reaction coordinate, after the channel has switched to the active conformation.

discussion

In this paper, we have investigated the effects of mutations at position 604 in the binding domain and of the olfactory amino terminal region on the kinetics at saturating concentrations of three different ligands. We have shown that direct interactions between the cyclic nucleotide and the amino acid at position 604 occur during both the opening and closing transitions of the allosteric conformational change. In contrast, the substitution of the olfactory for the rod amino terminal region appears to affect only the closing rate constant, suggesting that the favorable interdomain interactions that form when the auto-excitatory domain is present occur almost entirely after the channel has switched to the open conformation.

A molecular mechanism for the binding of cyclic nucleotides to CNG channels has been proposed, based on the CAP structure (Gordon and Zagotta, 1995b; Varnum et al., 1995). In this mechanism, the cyclic nucleotide–binding site is exposed when the channel is in the closed configuration because the C helix is rotated away from the β roll. The cyclic nucleotide then binds to the closed channel primarily through interactions between the β roll and the ribose and phosphate of the cyclic nucleotide. Activation involves a conformational change in the channel protein. At the level of the binding site, the conformational change is thought to involve movement of the β roll relative to the C helix, permitting residues in the C helix, in particular D604, to interact specifically with the purine ring of the bound cyclic nucleotide. For cGMP, it was proposed that the negatively charged carboxylic acid

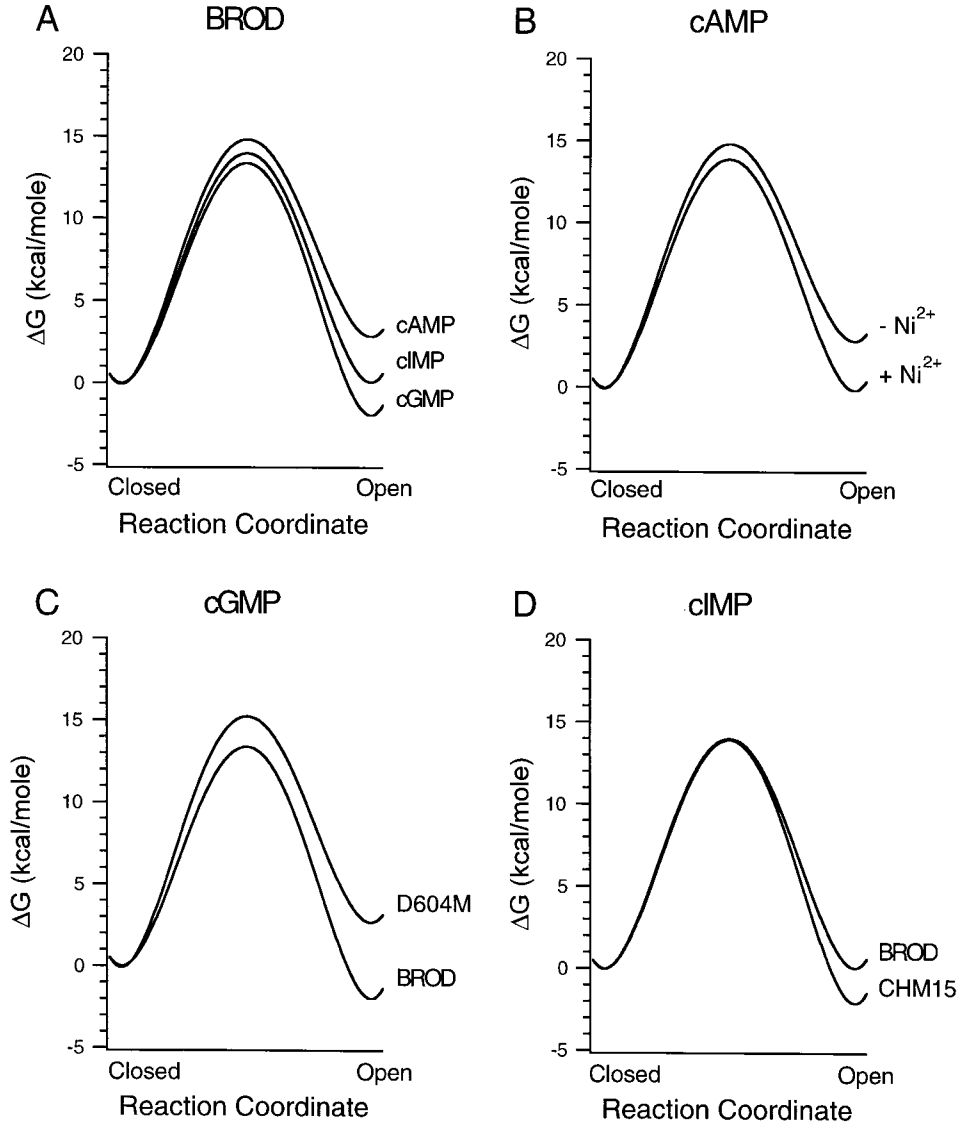

FIGURE 15. Free energy profile for the allosteric transition. The free energy profiles for the allosteric transition ($C_0 \leftrightarrow O_1$) are illustrated based on the median values of the rate constants determined from HMM analysis of the single-channel currents. The rate constants were converted to energies using simple transition-state theory, with the highest energy intermediate postulated to break down to product at the vibrational frequency of a covalent bond. (A) Free energy profiles for cGMP, cIMP, and cAMP on BROD channels. (B) Free energy profiles for cAMP with and without Ni^{2+}. (C) The free energy profiles of the allosteric transition for BROD and BROD-D604M channels activated by a saturating concentration of cGMP. (D) The free energy profiles of the allosteric transition for BROD and CHM15 channels activated by a saturating concentration of cIMP.

side chain of D604 in the C helix forms a pair of hydrogen bonds with the N1 and N2 hydrogen atoms on the guanine ring. This type of hydrogen bonding has been shown to occur in solution (Lancelot and Hélène, 1977) and in high affinity GTP binding proteins such as the α subunit of transducin (Noel et al., 1993), elongation factor EF-Tu (Jurnak, 1985), and H-Ras (Pai et al., 1989). This molecular mechanism is not unique, and we cannot completely rule out that substituents on the purine ring do not alter the chemical properties of the ring, or that mutations at D604 do not have indirect effects on the structure of the cyclic nucleotide–binding site. However, given the large body of data in support of a direct interaction between D604 and the purine ring, we have chosen to interpret our results in terms of this mechanism.

Based on the results of this investigation, the kinetic and molecular aspects of this mechanism for the allosteric transition have been refined. In particular, we have determined the rate constants at which the interactions are forming and unforming, and we now know the relative effects on the opening and closing transitions for each of the modifications studied. For the case of cGMP, we conclude that the pair of hydrogen bonds between the guanine ring and the aspartate is partially formed at the time of the transition state for the allosteric transition. Thus, the activation of the channel involves the formation of these two hydrogen bonds, and the closing of the channel involves the dissolution of these hydrogen bonds. This observation indicates that the formation of these hydrogen bonds is intimately involved in the allosteric transition, not an event that occurs before or immediately after it. For cIMP, we conclude that the formation of a hydrogen bond between D604 and the inosine moiety is also intimately involved in the allosteric transition, but the energies are approximately half those of cGMP, indicating a molecular mechanism where only a single hydrogen bond forms

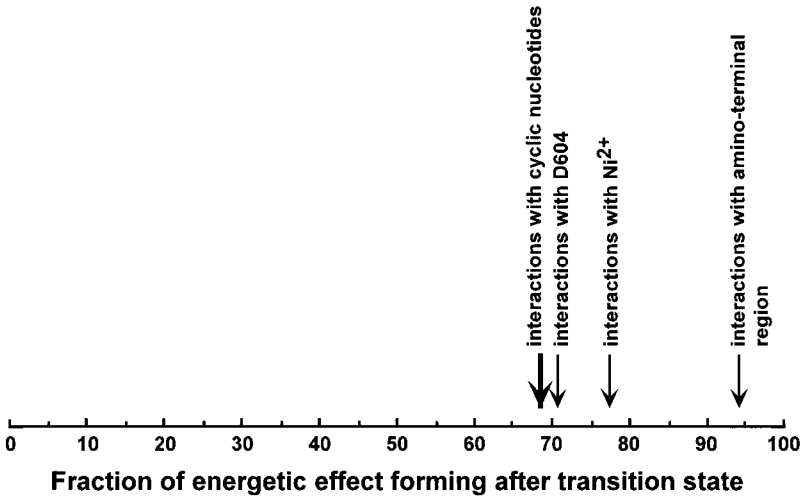

FIGURE 16. Fraction of energetic effect occurring after the allosteric transition. The fraction of the energetic effect occurring after the allosteric transition was calculated as $\Delta\Delta G^{\ddagger}/\Delta\Delta G^{0} = |(\Delta G^{\ddagger}_{1} - \Delta G^{\ddagger}_{2})/(\Delta G^{0}_{1} - \Delta G^{0}_{2})|$, where $\Delta G^{\ddagger}$ is the activation energy for the closing transition, ΔG^{0} is the standard free energy for the allosteric transition, and the subscript indicates the different conditions of allosteric modulation. ΔGs were the median values determined from an HMM analysis of the single-channel currents. The $\Delta\Delta G^{\ddagger}/\Delta\Delta G^{0}$ for the interactions with different cyclic nucleotides was the average of the values for BROD channels between cGMP and cIMP, cGMP and cAMP, and cIMP and cAMP. The $\Delta\Delta G^{\ddagger}/\Delta\Delta G^{0}$ for the interactions with D604 was the average of the values between BROD channels and D604M channels and between CHM15 channels and CHM15-D604M channels for all three cyclic nucleotides. The $\Delta\Delta G^{\ddagger}/\Delta\Delta G^{0}$ for the interactions with Ni^{2+} was the average of the values between BROD channels with and without Ni^{2+} for cIMP and cAMP (Sunderman and Zagotta, 1999). The $\Delta\Delta G^{\ddagger}/\Delta\Delta G^{0}$ for the interactions with the amino terminal region was the average of the values between BROD channels and CHM15 channels for all three cyclic nucleotides.

per subunit. The open probability increased for activation by cAMP when D604 was mutated to a polar uncharged residue, suggesting that interactions between the adenine ring and D604 destabilize the allosteric transition. Thus, other portions of the cyclic nucleotide and interactions not investigated here may explain the fact that cAMP is an agonist, not an antagonist, of the BROD channel. Alternatively, D604 may interact weakly with the adenine ring and less polar residues may interact more strongly.

Our analysis of the effect of the olfactory amino terminal region on channel activation indicates that the amino terminal region exerts its auto-excitatory effect late in the reaction coordinate and that the effects of the olfactory amino terminal region are cyclic nucleotide-independent. Previously, it has been shown that the rat olfactory CNG channel amino terminal region promotes channel activation by directly interacting with the carboxyl terminal gating machinery (Varnum and Zagotta, 1997). This mechanism was proposed based on in vitro binding assays and occurred even in the absence of cyclic nucleotide. The results of this investigation indicate that the affinity of the two terminal regions is only 2 kcal/mol higher for the open than the closed state. Since this energy difference is small, the most likely interpretation is that the two regions interact with high affinity both when the channels are open and closed and that the 2 kcal/mol energetic stabilization reflects the formation of a few hydrogen bonds per subunit or the removal of a few unfavorable interactions and not the binding or unbinding of the two terminal regions with each transition. Thus, our results refine the molecular mechanism of action by suggesting that the stabilization exerted by the amino terminal region occurs primarily after the transition state for the allosteric transition and occurs later in the reaction coordinate than the interactions between the cyclic nucleotides and the amino acid at position 604.

We thank Heidi Utsugi and Kevin Black for technical assistance, Fred Sigworth and Lalitha Venkataramanan for helpful discussions, and Richard W. Aldrich and Anita Zimmerman for comments on the manuscript.

This work was supported by the Howard Hughes Medical Institute and by a grant from the National Eye Institute (EY10329) to W.N. Zagotta. W.N. Zagotta is an investigator of the Howard Hughes Medical Institute.

Original version received 11 November 1998 and accepted version received 10 March 1999.

references

Altenhofen, W., J. Ludwig, E. Eismann, W. Kraus, W. Bonigk, and U.B. Kaupp. 1991. Control of ligand specificity in cyclic nucleotide–gated channels from rod photoreceptors and olfactory epithelium. *Proc. Natl. Acad. Sci. USA.* 88:9868–9872.

Carter, P.J., G. Winter, A.J. Wilkinson, and A.R. Fersht. 1984. The use of double mutants to detect structural changes in the active site of the tyrosyl-tRNA synthetase (*Bacillus stearothermophilus*). *Cell.* 38:835–840.

Chen, T.Y., and K.W. Yau. 1994. Direct modulation by Ca(2+)-calmodulin of cyclic nucleotide–activated channel of rat olfactory re-

ceptor neurons. *Nature.* 368:545–548.
Creighton, T.E. 1993. Proteins: structures and molecular properties. W.H. Freeman and Co., New York. 507 pp.
Eyring, H. 1935. The activated complex in chemical reactions. *J. Chem. Phys.* 3:283–291.
Fersht, A.R., J.P. Shi, J. Knill-Jones, D.M. Lowe, A.J. Wilkinson, D.M. Blow, P. Brick, P. Carter, M.M. Waye, and G. Winter. 1985. Hydrogen bonding and biological specificity analysed by protein engineering. *Nature.* 314:235–238.
Gordon, S.E., J.C. Oakley, M.D. Varnum, and W.N. Zagotta. 1996. Altered ligand specificity by protonation in the ligand binding domain of cyclic nucleotide–gated channels. *Biochemistry.* 35: 3994–4001.
Gordon, S.E., M.D. Varnum, and W.N. Zagotta. 1997. Direct interaction between amino- and carboxyl-terminal domains of cyclic nucleotide–gated channels. *Neuron*. 19:431–441.
Gordon, S.E., and W.N. Zagotta. 1995a. A histidine residue associated with the gate of the cyclic nucleotide–activated channels in rod photoreceptors. *Neuron*. 14:177–183.
Gordon, S.E., and W.N. Zagotta. 1995b. Localization of regions affecting an allosteric transition in cyclic nucleotide–activated channels. *Neuron*. 14:857–864.
Goulding, E.H., G.R. Tibbs, and S.A. Siegelbaum. 1994. Molecular mechanism of cyclic-nucleotide–gated channel activation. *Nature.* 372:369–374.
Hidalgo, P., and R. MacKinnon. 1995. Revealing the architecture of a K^+ channel pore through mutant cycles with a peptide inhibitor. *Science.* 268:307–310.
Horovitz, A., L. Serrano, B. Avron, M. Bycroft, and A.R. Fersht. 1990. Strength and cooperativity of contributions of surface salt bridges to protein stability. *J. Mol. Biol.* 216:1031–1044.
Jackson, M.B. 1993. On the time scale and time course of protein conformational changes. *J. Chem. Phys.* 99:7253–7259.
Jurnak, F. 1985. Structure of the GDP domain of EF-Tu and location of the amino acids homologous to ras oncogene proteins. *Science.* 230:32–36.
Kaupp, U.B., T. Niidome, T. Tanabe, S. Terada, W. Bonigk, W. Stühmer, N.J. Cook, K. Kangawa, H. Matsuo, T. Hirose, et al. 1989. Primary structure and functional expression from complementary DNA of the rod photoreceptor cyclic GMP-gated channel. *Nature.* 342:762–766.
Kumar, V.D., and I.T. Weber. 1992. Molecular model of the cyclic GMP-binding domain of the cyclic GMP-gated ion channel. *Biochemistry.* 31:4643–4649.
Lancelot, G., and C. Hélène. 1977. Selective recognition of nucleic acids by proteins: the specificity of guanine interaction with carboxylate ions. *Proc. Natl. Acad. Sci. USA.* 74:4872–4875.
Liu, D.T., G.R. Tibbs, and S.A. Siegelbaum. 1996. Subunit stoichiometry of cyclic nucleotide–gated channels and effects of subunit order on channel function. *Neuron*. 16:983–990.
Liu, M., T.Y. Chen, B. Ahamed, J. Li, and K.W. Yau. 1994. Calcium-calmodulin modulation of the olfactory cyclic nucleotide–gated cation channel. *Science.* 266:1348–1354.
McKay, D.B., and T.A. Steitz. 1981. Structure of catabolite gene activator protein at 2.9 Å resolution suggests binding to left-handed B-DNA. *Nature*. 290:744–749.
Noel, J.P., H.E. Hamm, and P.B. Sigler. 1993. The 2.2 Å crystal structure of transducin-alpha complexed with GTP gamma S. *Nature.* 366:654–663.
Pai, E.F., W. Kabsch, U. Krengel, K.C. Holmes, J. John, and A. Wittinghofer. 1989. Structure of the guanine-nucleotide-binding domain of the Ha-ras oncogene product p21 in the triphosphate conformation. *Nature.* 341:209–214.
Serrano, L., A. Horovitz, B. Avron, M. Bycroft, and A.R. Fersht. 1990. Estimating the contribution of engineered surface electrostatic interactions to protein stability by using double-mutant cycles. *Biochemistry.* 29:9343–9352.
Shabb, J.B., B.D. Buzzeo, L. Ng, and J.D. Corbin. 1991. Mutating protein kinase cAMP-binding sites into cGMP-binding sites. Mechanism of cGMP selectivity. *J. Biol. Chem.* 266:24320–24326.
Sunderman, E.R., and W.N. Zagotta. 1999. Mechanism of allosteric modulation of rod cyclic nucleotide–gated channels. *J. Gen. Physiol.* 113:601–619.
Varnum, M.D., K.D. Black, and W.N. Zagotta. 1995. Molecular mechanism for ligand discrimination of cyclic nucleotide–gated channels. *Neuron*. 15:619–625.
Varnum, M.D., and W.N. Zagotta. 1996. Subunit interactions in the activation of cyclic nucleotide–gated channels. *Biophys. J.* 70: 2667–2679.
Varnum, M.D., and W.N. Zagotta. 1997. Interdomain interactions underlying activation of cyclic nucleotide–gated channels. *Science.* 278:110–113.
Weber, I.T., and T.A. Steitz. 1987. Structure of a complex of catabolite gene activator protein and cyclic AMP refined at 2.5 A resolution. *J. Mol. Biol.* 198:311–326.
Zagotta, W.N., T. Hoshi, and R.W. Aldrich. 1989. Gating of single *Shaker* potassium channels in *Drosophila* muscle and in *Xenopus* oocytes injected with *Shaker* mRNA. *Proc. Natl. Acad. Sci. USA.* 86: 7243–7247.